

PAPER

Analysis and validation of mathematical models of secondary velocities along vertical and transverse directions in wide open-channel turbulent flows

To cite this article: Snehasis Kundu and Titas Chattopadhyay 2022 *Fluid Dyn. Res.* **54** 015515

View the [article online](#) for updates and enhancements.

You may also like

- [Testing and analysis of magnetorheological fluid sedimentation in a column using a vertical axis inductance monitoring system](#)
Young-Tai Choi, Lei Xie and Norman M Wereley
- [Vertical distribution of fluid velocity and suspended sediment in open channel turbulent flow](#)
Debasish Pal and Koeli Ghoshal
- [Semi-analytical solution for one-dimensional unsteady sediment transport model in open channel with concentration-dependent settling velocity](#)
Shiv Mohan, Manotosh Kumbhakar, Koeli Ghoshal et al.

Analysis and validation of mathematical models of secondary velocities along vertical and transverse directions in wide open-channel turbulent flows

Snehasis Kundu*  and Titas Chattopadhyay 

Department of Mathematics, NIT Jamshedpur, Jamshedpur, Jharkhand, 831014, India

E-mail: snehasis.math@nitjsr.ac.in

Received 9 December 2021; revised 12 February 2022

Accepted for publication 15 February 2022

Published 4 March 2022

Communicated by Professor Koji Nagata



Abstract

Cellular secondary flows are inevitably present in turbulent flows through ducts, natural or artificial channels, and compound channels. Secondary currents significantly modify the characteristics of turbulent quantities, the pattern of primary flow velocity by causing dip-phenomenon. To understand the detailed mechanism and hidden cause, modelling of secondary flow velocities is crucial. In this study, proper mathematical models of secondary flow velocities along vertical and transverse directions are proposed for steady and uniform turbulent flow through wide open channels with equal smooth and rough bed strips. Starting from the continuity and the Reynolds averaged Navier–Stokes equations, governing equation for secondary velocity is derived first and then using appropriate boundary conditions (no-slip boundary conditions at channel bottom and free surface, and maximum vertical velocity in magnitude at the interface of two cellular secondary cells and at mid-depth of the channel. All these conditions are consistent with several experimental observations). A new model of the streamwise Reynolds shear stress is proposed for the entire cross-sectional plane and using it, the analytical solutions are obtained. Proposed models include the effects of viscosity of the fluid and the eddy viscosity model of turbulence. All suggested models are validated with existing experimental data in rectangular open-channel flows, compound open channel flows, and duct flows, and satisfactory results are obtained. Furthermore, models are also compared with existing empirical models from literature to show the effectiveness and superiority of proposed models. Apart from these, the

* Author to whom any correspondence should be addressed.

obtained results from this study are used to investigate the effects of vertical and transverse secondary flow velocities on the settling velocity vector in a cross-sectional plane. Effective alternative models for the settling velocity vector are suggested. The model of settling velocity vector is also compared with the existing model. Finally, all results are justified from physical viewpoints.

Keywords: open channel turbulent flow, secondary currents, Reynolds shear stress, settling velocity vector, method of separation of variables

1. Introduction

Turbulent flows in rivers and open channels are natural phenomena that have drawn the attention of painters, scientists, and engineers through decades. Open channel flows are three dimensional and are often too complex to represent or approximate as two dimensional flows (Bradshaw 1987). Therefore, consideration of secondary currents along vertical and transverse direction is crucial for the understanding of transfer and mixing mechanisms under the influence of turbulence. Streamwise helical circulations are known as secondary flows which can occur due to different reasons. These secondary currents significantly affect the distribution of primary flow velocity (Guo 1998, Guo and Julien 2001, 2008, Yang *et al* 2004, Absi 2010, Kundu and Ghoshal 2012); Reynolds shear stress (Yang *et al* 2004, Yang 2005); suspension concentration of sediment particles (Wang and Cheng 2008, Kundu and Ghoshal 2014, Kundu 2015); bed shear stress (Nezu and Nakagawa 1993, Wang and Cheng 2005) and particle settling velocity (Wang and Cheng 2008) in the vertical and transverse directions. The effects of secondary flow on the distribution of the Reynolds shear stress, settling velocity are little-known compared to its effects on the primary velocity distribution due to lack of proper mathematical understanding and models of secondary flows. On the other hand, Wang and Cheng (2006) reported that the time mean structure of secondary current significantly changes due to different bed configurations. Apart from these, in sediment-laden flow, viscosity considerably changes along vertical and spanwise direction which may reduce the flow circulations. As a consequence, proper modelling of secondary flow velocities (in the vertical and transverse direction) including effects of fluid viscosity and different bed configurations is necessary to understand the pattern of secondary current and to have proper knowledge of its effects on the above mentioned flow quantities.

Prandtl (1926) classified the secondary currents into two categories depending on their underlying generation mechanism as: secondary current of the first kind and secondary current of the second kind. Prandtl's secondary current of first kind is observed in curved pipe, river bends and meandering channels and they are driven by centrifugal force or pressure gradient along transverse direction. The second kind of Prandtl's secondary current is generated as a result of turbulence non-homogeneity and anisotropy. Streamwise vortices are developed as a result of transverse variance of the turbulent stresses. These vortices further extend along the transverse direction and cause a flow circulation with dimension of the flow depth (Wang and Cheng 2006). This type of secondary current is observed in turbulent flow through straight wide and narrow open channels. Often, this type of secondary current is called as turbulence-induced secondary current. Among different variety of turbulence-induced secondary currents, in this study secondary currents associated to different bed roughness configurations in wide channels are investigated theoretically. The existence of secondary current in open channel turbulent flows have been discovered by several researchers (Thomson 1876, Francis 1878,

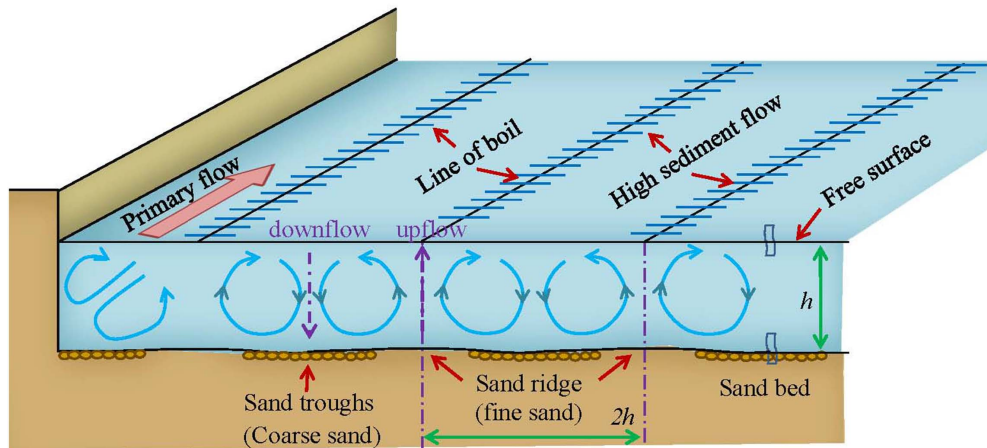


Figure 1 . Schematic diagram of secondary currents in wide channels with line of boil or high sediment zones.

Stearns 1883, Gibson 1909, Vanoni 1946, Coleman 1969). Gibson and Rodi (1982) envisaged the pattern of secondary current in a narrow open channel which are called as ‘corner’-induced secondary current (Gessner 1973). In 1980s, several researchers found that secondary current can also be generated without ‘corner flows’, if the channel bed is slightly perturbed. Nezu and Rodi (1985) experimentally showed that lateral variations in bed topography and roughness can lead to the formation of secondary currents, which are independent of the side-wall effect or the corner induced secondary current (Nezu and Nakagawa 1993, Wang and Cheng 2005). Besides these reasons, also it has been shown that this kind of secondary current may be formed in buoyancy-driven flow even in straight circular pipes (Hallez and Magnaudet 2009), where bed roughness and bed topography do not play any role. Further, Kinoshita (1967) postulated the form of streamwise secondary currents in straight rivers. He suggested that streamwise secondary currents consists of two counter-rotating large vortices with diameter equal to flow depth and spanwise spacing of twice the flow depth. A schematic diagram is presented in figure 1. During the initiation of flow, due to change of bed roughness along lateral direction cellular secondary currents are gradually developed. Further sediment beds are continuously deformed and eventually forms ‘sand troughs’ (made of coarse sand which can be regarded as rough bed surface) and ‘sand ridges’ (made of fine sands and can be regarded as smooth bed surface). These cellular secondary cells consist of upflow and downflow zones. The upflow and downflow zones are correspond to smooth and rough bed surfaces respectively Wang and Cheng (2005, 2006) (see figure 1). These spanwise upflow and downflow of secondary currents change the distributions of turbulent stresses and primary flow velocities. Yang and his co-researchers Yang *et al* (2004), Yang (2005, 2007), Kundu and Ghoshal (2012) showed that in the presence of vertical secondary currents, the distribution of the Reynolds shear stress deviates from its traditional linear type profile. They also showed that zero Reynolds shear stress always corresponds to the velocity-dip-position which appears beneath the free surface and as a consequence, the maximum primary flow velocity occurs below the free surface. Kundu and Ghoshal (2012) showed that with the increase of vertical secondary flow velocity (measured through the dip-correction parameter), zero-shear

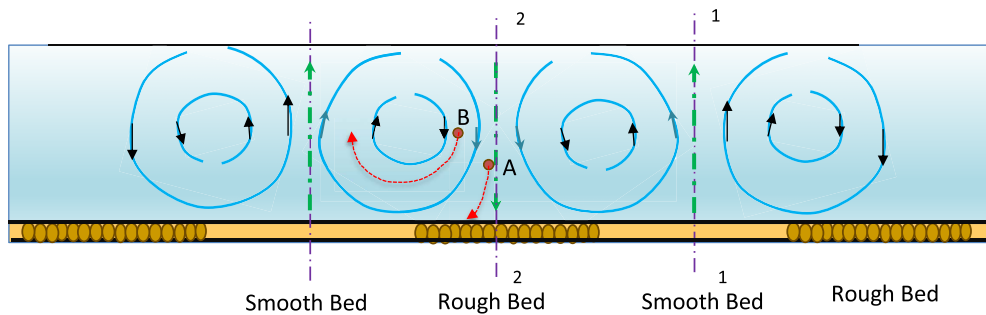


Figure 2. Schematic diagram for effect of secondary currents on settlement of particles.

stress point gradually shifts downward from free surface. Moramarco and Singh (2004) pointed out that measured maximum primary velocity usually appears below the free surface at a distance of 0.05–0.5 of the flow depth. In the Mississippi River, maximum velocity appears at two-third of the water depth from the channel bottom (Gordon 1992). Later Wang and Cheng (2005) performed experiments to investigate the effects of secondary flows on bed shear stress and streamwise Reynolds distribution in wide artificial open channels. Their finding suggests that the Reynolds shear stress shows a convex profile in the upflow zones and a concave profile in the downflow zone. Apart from the primary velocity, Wang and Cheng (2008) investigated the effects of cellular secondary flow on settling velocity vectors. They found that the pattern of contour lines (open or closed) of settling velocity vectors depends on the ratio V_{\max}/ω_0 (where V_{\max} is the maximum upwelling velocity and ω_0 is the particle settling velocity in still water). A schematic diagram is presented in figure 2 to demonstrate the interplay between secondary current and settlement of particles. In the figure, two vertical sections (namely 1-1 and 2-2) are considered. Along the section 1-1, secondary flow velocity is along upward direction and it is along the downward direction along the section 2-2. Two particles A and B are considered at pointed locations in the figure for the description. Particle A which is present along the section 2-2, moves along downward direction under the influence of downward flow velocity and eventually may settle on the bed surface or slide along transverse direction (Kundu 2016). On the other hand, particle B is trapped between two consecutive closed secondary streamlines. Due to the continuous circulations of secondary flows in that zone, it may carry particle B upwards in spite of gravity due to its upward motion. The possible paths of particles A and B are shown in the figure with red dotted lines. These clearly indicate the role of secondary currents on the movement of settlement of particles.

A number of researchers investigated the structure of secondary currents and proposed empirical, analytical and numerical models under different flow conditions and bed configurations. Ikeda (1981) proposed models to predict secondary flow velocities. The effects of fluid viscosity and unequal bed configuration are not included in the study. The application and results of this study are limited as the Reynolds shear stress is considered as linear model which rarely holds in such flows (Yang *et al* 2004). The solutions of Ikeda (1981) were analyzed by Nezu and Nakagawa (1993). Nezu and Nakagawa (1993) found that the models of Ikeda (1981) represent the ideal flow situations only and may be applicable for unequal bed roughness configurations. Instead of proposing a model, Chiu and Lin (1983), Chiu and Chiu (1985) suggested a method to calculate secondary current from the primary velocity. In their

method, the rectangular coordinate system is transformed into a special curvilinear coordinate system which makes the computation process complicated and give rise to large errors. Since the value of secondary flow velocities are quite small compared to the magnitude of primary flow velocity, the models of Chiu and Lin (1983), Chiu and Chou (1985) are not suitable. Later, Kotsovinos (1988) proposed mathematical models of secondary flow velocities by presenting a possible mechanism which produces the cellular secondary current in duct flows. Wang and Cheng (2006) performed experiments to investigate the time mean structures of secondary flows in wide open channel with different longitudinal bed forms. From experimental observations of secondary streamlines, they empirically postulated a simple analytical formula for the stream function. This empirical result was previously obtained by Kotsovinos (1988) in duct flows. Apart from it, Wang and Cheng (2006) also observed that the cellular shape of secondary cells changes under different bed roughness configurations. More precisely they reported three different types of shapes of secondary cells as: cellular, laterally skewed and vertically distorted. For each of these shapes, they empirically proposed the forms of stream function using suitable boundary conditions and the property of periodic functions. Based on this empirical form of the stream function, they derived models of secondary flow velocities along vertical and transverse directions. In their studies, Yang (2005) and Yang *et al* (2012) empirically proposed parabolic type model for the vertical secondary velocity using boundary conditions. Later Kundu and Ghoshal (2013) extended the study of Yang (2005) for sediment-laden flows and proposed a general empirical model for vertical secondary flow velocity. The model of Kundu and Ghoshal (2013) is used to study the effects of secondary current on suspension distribution. In the same year, Ghoshal *et al* (2013) performed experimental study on gravel mixture bed. They found that a beta density function satisfies the obtained experimental data of vertical velocity well. This model is based on experimental findings and is proposed empirically without any reasonable mathematical description. A list of all the aforementioned empirical/semi empirical model of secondary flow velocities is presented in table 1 with their origin and limitations for better understanding. Apart from these analytical empirical models, several studies have been carried out using numerical simulations to investigate secondary currents. Gessner and Emery (1981) investigated secondary flows numerically for a duct flow. Further, Lin, Yu *et al* (2017) and Lin, Shao *et al* (2017) studied the effects of presence of finite-size neutrally buoyant and heavy particles on mean secondary flows respectively. Their results for neutrally buoyant particles show that the mean secondary flow is enhanced and its circulation centre shifts closer to the centre of the duct cross section when the neutrally buoyant and heavy particles are added. They postulated that due to the presence of particles, gradients of the secondary Reynolds normal stress difference and shear stress in the near-wall region near the corners, enhances which results an increase in mean secondary flow. Soualmia *et al* (2008) performed numerical studies for turbulent characteristics using $k - \varepsilon$ models. Recently, Proust and Nikora (2020) performed experimental studies to investigate transverse secondary current in a compound open channel. Though the numerical models proposed in these studies can predict secondary velocities, but they are computationally complex and costly. From aforementioned discussions it can be understood that previous investigations mostly propose empirical models for the secondary flow velocities and employ them to investigate primary flow velocity, the Reynolds shear stress and suspension concentration distribution. Though in few studies models are derived by solving governing equations, but effects of the Reynolds shear stress and fluid viscosity are neglected. As a result, most of these models have limitations and drawbacks. Apart from these, the models summarized in table 1, are applicable only in open channel flows. Thus, more general models are required which can be simultaneously applicable for compound channel flows and duct flows apart from wide open channel flows.

Table 1. Details and limitations of empirical and semi-empirical models in literature.

Authors	Empirical/ semi-empirical/ proposed model	Remarks and limitations
Ikeda (1981)	$\frac{r}{\bar{u}_*} = -\frac{6A_b}{\kappa\pi^2} \cos(\pi\tilde{y})$ $[(2\tilde{z} - 1) \cos(\pi\tilde{z}) + 1],$ $\frac{q}{\bar{u}_*} = \frac{6A_b}{\kappa\pi^2} \sin(\pi\tilde{y})$ $\left[\frac{2}{\pi} \cos(\pi\tilde{z}) - (2\tilde{z} - 1) \sin(\pi\tilde{z}) \right]$	Used simplified RANS equation and solved it. This model does not contain effect of viscosity and only applied in open channel flows.
Kotsovinos (1988)	$r = -A \cos(\pi\tilde{y}) \sin(\pi\tilde{z}),$ $q = A \sin(\pi\tilde{y}) \cos(\pi\tilde{z})$	Derived from momentum equations assuming linear stability. Effects of bed roughness and viscosity effects are not included. Proposed only for open channel flows.
Wang and Cheng (2006)	$\frac{r}{W_{\max}} = -\cos(\pi\tilde{y}) \sin(\pi\tilde{z}),$ $\frac{q}{W_{\max}} = \sin(\pi\tilde{y}) \cos(\pi\tilde{z})$	Semi-empirical model proposed based on the empirical form of the stream function.
Yang (2005), Yang <i>et al</i> (2012)	$\frac{r}{u_*} = \alpha \kappa \tilde{z}^m (1 - \tilde{z})^n,$ $n \text{ are empirical coefficients}$	Empirical model. The model is proposed on the basis of the boundary conditions: at bed, $z = 0, w = 0$ and at free surface $z = h, w = 0$. It depends only on vertical coordinate z .
Kundu and Ghoshal (2013)	$\frac{r}{u_*} = \alpha \kappa \tilde{z}^m (1 - \tilde{z})^n (1 - C)^p,$ $C \text{ is concentration}$	The model is empirically proposed for sediment-laden flow. No rigorous mathematical background is present.
Ghoshal <i>et al</i> (2013)	$\frac{r}{u_*} = b_0 \frac{\Gamma(b_1 + b_2)}{\Gamma(b_1)\Gamma(b_2)} \tilde{z}^{b_1-1}$ $(1 - \tilde{z})^{b_2-1}$	Model is empirically proposed based on the experimental data rather than theoretical perspective.

The main objectives of this study are: (a) to find general and appropriate mathematical models for the vertical and transverse secondary flow velocities in wide open channels, compound channels and ducts including effects of viscosity of fluid, eddy viscosity and modified streamwise Reynolds shear stress distribution; (b) to derived these models from a mathematical viewpoint rather empirically proposed them; (c) to validate obtained models with wide range of experimental data for open channel flow, compound channel flow and duct flow; (d) to compare the proposed models with previous empirical models; and (e) to reinvestigate the

effects of secondary currents on settling velocity vectors employing the obtained models from this study.

2. Derivation of governing equation

To derive the full governing equation, we consider a steady and uniform turbulent flow through straight wide open channels with longitudinal bedforms. The bedforms considered here have symmetric pattern about the centerline and composed of smooth and rough bed strips of equal length along transverse direction. We consider x -axis along the main flow direction along which the flow is considered as uniform. The lateral and vertical coordinates are considered along y and z directions respectively. Mean flow velocity components along x , y and z directions are given by p , q and r respectively. Under such flow condition, equations of motion for the analysis of secondary currents are governed by Reynolds averaged continuity and Navier–Stokes (RANS) equations which are expressed as follows

$$\frac{\partial q}{\partial y} + \frac{\partial r}{\partial z} = 0 \quad (1)$$

and

$$\frac{\partial q}{\partial t} + q \frac{\partial q}{\partial y} + r \frac{\partial q}{\partial z} = -\frac{1}{\rho} \frac{\partial P}{\partial y} + \nu \nabla^2 q + \left[\frac{\partial}{\partial y} (-\overline{q'^2}) + \frac{\partial}{\partial z} (-\overline{q'r'}) \right] \quad (2)$$

$$\frac{\partial r}{\partial t} + q \frac{\partial r}{\partial y} + r \frac{\partial r}{\partial z} = -gJ - \frac{1}{\rho} \frac{\partial P}{\partial z} + \nu \nabla^2 r + \left[\frac{\partial}{\partial y} (-\overline{q'r'}) + \frac{\partial}{\partial z} (-\overline{r'^2}) \right] \quad (3)$$

where J is the longitudinal channel slope, g is gravitational acceleration, P is pressure, ρ is fluid density, ν is kinematic viscosity. Here primes denote the turbulent fluctuation part of corresponding velocity components. Since in this study, the Prandtl's secondary current of second kind is considered which is generated due to the turbulence non-homogeneity and anisotropy in open-channels, the effect of pressure gradient can be neglected. Therefore, eliminating the pressure term and defining vorticity vector $\Omega = \frac{\partial r}{\partial y} - \frac{\partial q}{\partial z}$, above momentum equations can be combined as

$$\begin{aligned} \frac{\partial}{\partial t} \left(\frac{\partial r}{\partial y} - \frac{\partial q}{\partial z} \right) + \underbrace{q \frac{\partial \Omega}{\partial y} + r \frac{\partial \Omega}{\partial z}}_I &= \underbrace{\frac{\partial^2}{\partial y \partial z} (\overline{q'^2} - \overline{r'^2})}_{II} + \underbrace{\left(\frac{\partial^2}{\partial z^2} - \frac{\partial^2}{\partial y^2} \right) \overline{q'r'}}_{III} \\ &+ \underbrace{\nu \nabla^2 \left(\frac{\partial r}{\partial y} - \frac{\partial q}{\partial z} \right)}_{IV}. \end{aligned} \quad (4)$$

In equation (4) term I denotes the advection of vorticity under secondary flow velocities which establishes the existence of secondary current, terms under II and III denote generation of secondary current due to turbulent anisotropy and suppression of secondary current due to the Reynolds shear stress respectively (Nezu and Nakagawa 1993). Term IV is the viscous term. Among all these terms, terms II and III are dominant terms compared to term I (Nezu and Nakagawa 1984). Further if sediment particles are present in the flow, viscosity term IV plays significant role and therefore cannot be neglected as mentioned earlier. Also consideration of the term IV makes the model more general to apply in sediment-laden flows. Since the study focuses on Prandtl's secondary current of second type, term I is neglected as it is small

compared to other terms in the equation as proposed by (Ikeda 1981, Nezu and Nakagawa 1993).

Differentiation of equation (4) with respect to y and simplification gives the below governing equation

$$\left(\frac{\partial}{\partial t} - \nu \nabla^2\right) \nabla^2 r = \frac{\partial^3}{\partial y^2 \partial z} (\overline{q'^2} - \overline{r'^2}) + \left(\frac{\partial^2}{\partial z^2} - \frac{\partial^2}{\partial y^2}\right) \frac{\partial}{\partial y} (\overline{q'r'}) \quad (5)$$

where $\nabla^2 = \frac{\partial^2}{\partial y^2} + \frac{\partial^2}{\partial z^2}$ denotes the Laplacian operator. To find full analytical solution of equation (5) for the vertical component of secondary flow velocity r , algebraic closure of turbulent shear stress and normal stress are required. Several researchers considered equation (5) to investigate the secondary current in duct flow and straight wide channel flow without sediment bed. The focus of all previous studies was mainly on the balance between the generation and suppression of secondary terms. Brundrett and Baines (1964) and Tracy Tracy (1965) considered equation (5). In both these studies they found that, in a duct flow, the generation of secondary current is significantly higher than the suppression term and neglected suppression term in their studies. Later, Ikeda (1981) considered that the generation of secondary currents is balanced by the suppression of secondary current by the Reynolds shear stress with negligible viscosity and considered a more simplified equation of equation (5). Whereas the viscosity plays a significant role in sediment mixed flows. Due to the presence of particles in fluid, distribution of the eddy viscosity and the Reynolds shear stress changes. Therefore these aforementioned studies are not suitable to apply for investigation of secondary flows in rivers. In the present study it is assumed that generation of secondary current is balanced by the suppression by the Reynolds shear stress as well as by the viscous dissipation. The Reynolds shear stress $-\overline{q'r'}$ can be expressed by the eddy viscosity models as (Hinze 1975)

$$-\overline{q'r'} = \nu_t \left(\frac{\partial q}{\partial z} + \frac{\partial r}{\partial y} \right) \quad (6)$$

where ν_t denotes the eddy viscosity which are generally considered as constant in such studies after considering the logarithmic law of primary velocity as $\nu_t = (\kappa u_* h)/6$ (Ikeda 1981) in which u_* is the shear velocity. It is already reported in several studies that in such complex flows, the log-law cannot be applied for the primary flow velocity throughout the flow depth (Guo 2006, Kundu 2015). The log-law can predict the primary flow velocity in the inner region ($z/h < 0.2$) only. In the outer region ($z \geq 0.2h$), log-law deviates from the experimental data and also fails to predict the maximum velocity below the free surface which is known as dip-phenomena. Kundu and Ghoshal (2012) proposed the general model total-dip-modified-log-wake law (TDMLWL) which predicts velocity through the flow depth more accurately than such previous models. This model is simple and easy to apply due to its full analytical form. Therefore, to derive a more general model of eddy viscosity, the TDMLWL is employed in this study. Also, till now no suitable and appropriate model of two dimensional eddy viscosity is available in the literature and hence the depth averaged model of the eddy viscosity is employed in this study as a first approximation (It is important to point out that though this approximation is made, but the final results are good and not compromised.). Using it, the modified depth averaged eddy viscosity model is expressed (see appendix for detail calculation) as (Kundu and Ghoshal 2012)

$$\bar{\nu}_t = \kappa u_* h \int_0^1 \frac{\tilde{z}(1-\tilde{z})}{1+12\Pi\tilde{z}^2(1-\tilde{z})} d\tilde{z}. \quad (7)$$

The effects of normal shear stresses are reflected by term II in governing equation (4). This term signifies the vorticity or secondary flow generation term. The present study primarily

focuses is to predict the structures of secondary flow cells due to a periodic bed perturbation in wide open-channel more accurately. In the case of wide open channels, due to the bed effects, cellular secondary currents are generated that spread over the whole flow depth and width of the channel (Nezu and Rodi 1985). These secondary circulations in return modify the bed forms and bed configurations. Therefore, it can be assumed that the bed perturbation occurs over the whole width of the channel. Since these secondary flows are present over the whole flow domain, it is more reasonable to consider the vorticity generation term as universal rather than local. Therefore normal shear stress term can be assumed following Ikeda (1981) as

$$\frac{\overline{q'^2 - r'^2}}{u_*^2} = \alpha_0 \frac{\overline{-p'r'}}{u_*^2} \quad (8)$$

where α_0 is a constant generally considered as unity (Nezu and Nakagawa 1993). Apart from the above reason, equation (8) was also considered by several previous researchers (Perkins 1970, Townsend 1976, McLean 1981, Nakagawa *et al* 1981, Nezu and Nakagawa 1993) related to similar type of study. Equation (8) shows that the production of secondary current (SC) due to turbulent anisotropy is balanced by the suppression of secondary current due to Reynolds shear stress to make a balance of stability in the flow. Therefore, the constant α_0 can be regarded as the ratio of SC production to suppression of SC and it can be considered as a stability index. From physical point of view, $\alpha_0 > 1$ indicates the grow of SC and gradually flow becomes unstable, and $\alpha_0 < 1$ indicates a decay in the formation of SC and flow eventually becomes stable to rectilinear flow. In equation (8), further $\alpha_0 = 1$ signifies that stability to instability of the flow gradually occurs through the appearance of secondary flows (Kotsovinos 1988). Further, to find the appropriate closure of normal shear stress term in equation (8), the closure of the Reynolds shear stresses are to be considered. The Reynolds shear stresses are generally modeled by a linear profile which satisfy the boundary conditions as at $z = 0$, $\overline{-p'r'} = \tau_0 (= \rho u_*^2)$ and at $z = h$, $\overline{-p'r'} = 0$. Yang *et al* (2004) analyzed the Reynolds shear stress distribution considering effects of secondary current velocities to study primary flow velocity. After analyzing the data of Immamoto and Ishigaki (1988) (narrow channel experimental data with $Ar = 5$), he empirically proposed a modified linear type profile form of the Reynolds shear stress which includes the effect of vertical component of secondary current. The model of Yang *et al* (2004) was also considered in some studies by Yang (2007), Kundu and Ghoshal (2012), Yang *et al* (2012) for investigating turbulent velocity profiles. Whereas the experimental observations reported by Wang and Cheng (2005) in a wide open-channel flow show that the Reynolds shear stress distribution differs from the linear profile (which generally used in two dimensional flows) and exhibit upward convex and upward concave profiles over smooth and rough beds respectively. Figure 3 shows the relationship between the secondary circulation over smooth and rough bed strips with the distribution of the Reynolds shear stress $\overline{-p'r'}/u_*^2$ as observed by (Wang and Cheng 2005). It can be seen from figure 3(a) that it follows a non-linear profile along with the aforementioned boundary conditions. Secondary current flows along vertically upward direction along the section A at the middle of the smooth bed strip (where $\tilde{y} = -1.0$). Along the section B, the secondary current is directed along lateral direction (tangential direction of bed) and along the section C (which is the middle of rough bed strip), secondary flow occurs along vertically downward direction. Figure 3(b) shows that along the section A, the Reynolds shear stress increases and follows an upward convex profile; whereas along the section C, it decreases and shows an upward concave profile. The linear profile occurs only along the section B where no vertical component of the secondary current is present. Therefore for wide open channel flows with alternate bed forms, model of Yang *et al* (2004) needs to be modified. It is also reported by Wang and Cheng (2005) that the variation of

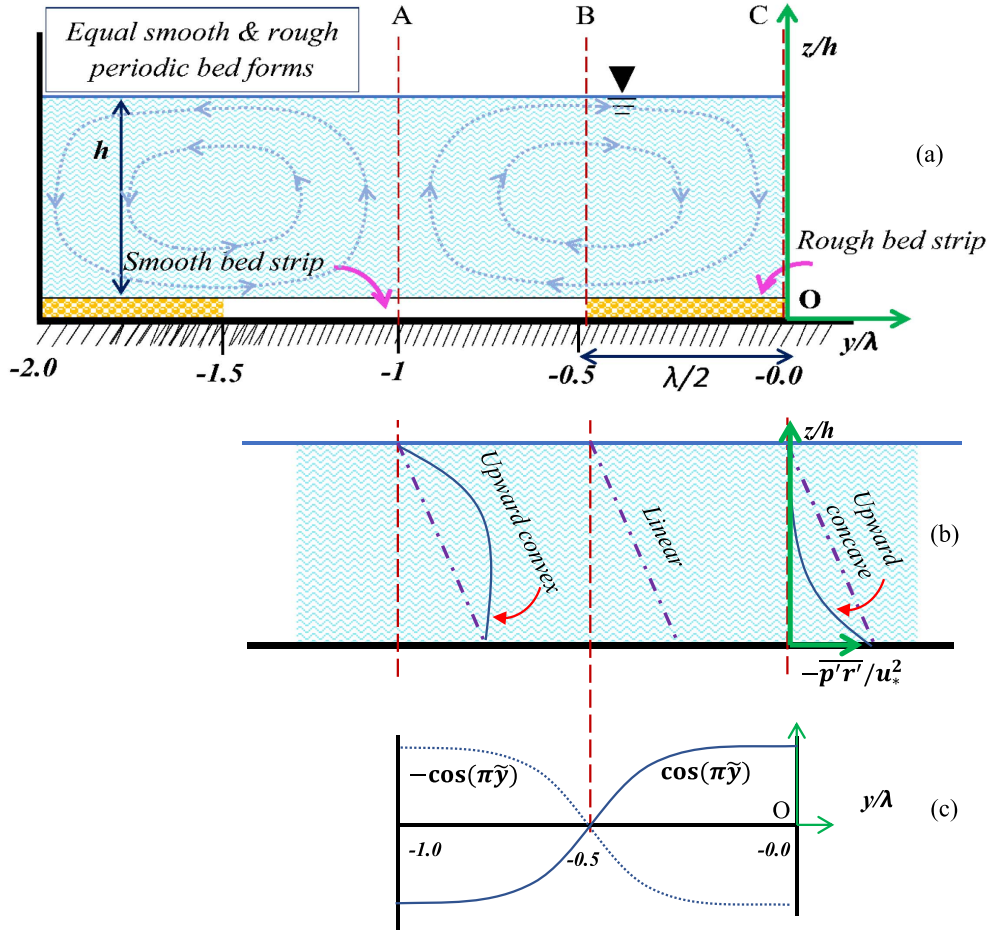


Figure 3. Relation between the secondary circulation and Reynolds shear stress ($-\overline{p'r'}/u_*^2$) distribution in wide open-channel with alternate rough and smooth bed forms (after Wang and Cheng (2005)).

the Reynolds shear stress from upward convex profile to upward concave profile occurs gradually along transverse direction. Figure 3(c) shows that the parameter α in the model of Yang *et al* (2004) can be modeled by a cosine function. Therefore in this study, the shear stresses due to turbulence is modeled after including these effects as

$$\frac{\overline{q'^2} - \overline{r'^2}}{u_*^2} = \alpha_0 \frac{\overline{-p'r'}}{u_*^2} = \alpha_0 \left[\left(1 - \frac{z}{h}\right) - \alpha \pi \cos\left(\frac{\pi y}{\lambda}\right) \left\{ \frac{z}{h} - \left(\frac{z}{h}\right)^2 \right\} \right] \quad (9)$$

where α is called as *dip correction parameter* which physically indicates the strength of secondary current and can be determined from experimental data. Figure 4 shows the validation of the proposed model with the experimental data of (Wang and Cheng 2005). Here the value of α is taken as 0.2, fixed for all channel sections and other values of parameters are taken form (Wang and Cheng 2005). It can be seen that proposed model reasonably agrees well with these data sets.

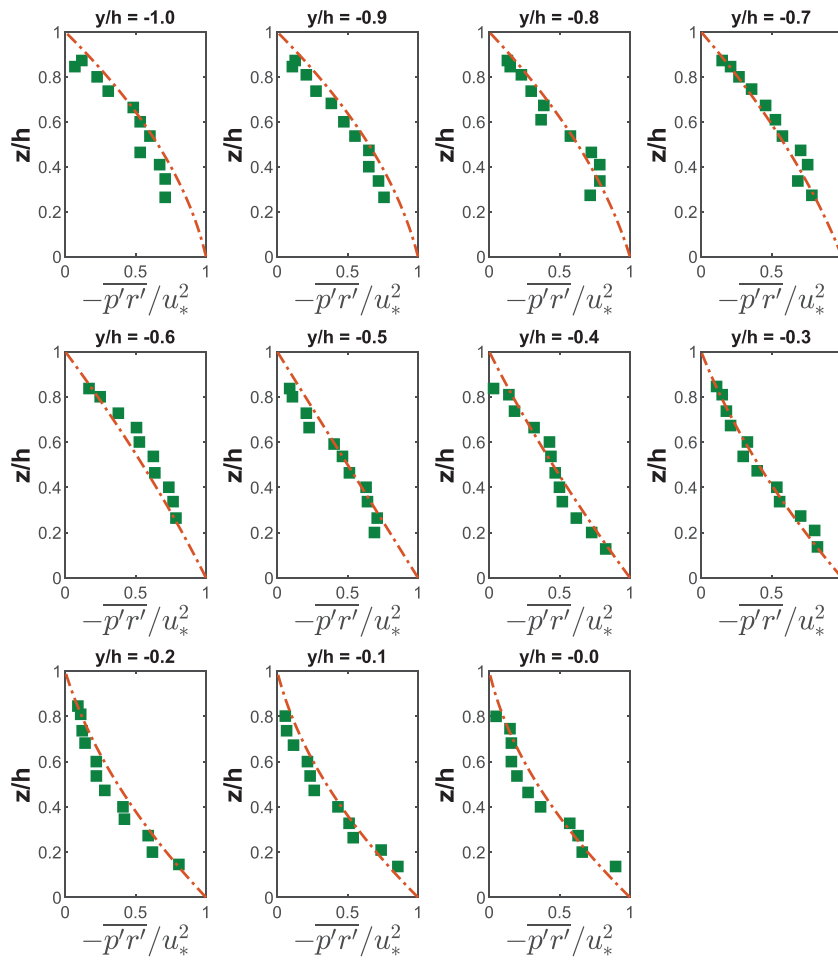


Figure 4. Validation of the proposed Reynolds shear stress model (equation (9)) with experimental data of Wang and Cheng (2005).

Substituting equations (6)–(9) into equation (5) and simplifying the governing equation is obtained as

$$\left(\frac{\partial}{\partial t} - \nu \nabla^2\right) \nabla^2 r = \phi(y, z) + \bar{\nu}_t \left(\frac{\partial^4 r}{\partial z^4} - 2 \frac{\partial^4 r}{\partial y^2 \partial z^2} + \frac{\partial^4 r}{\partial y^4}\right) \tag{10}$$

where $\phi(y, z)$ is a function of y and z defined as

$$\phi(y, z) = \frac{u_*^2}{\lambda^2 h} \alpha_0 \alpha \pi^3 \cos\left(\frac{\pi y}{h}\right) \left[1 - 2 \frac{z}{h}\right]. \tag{11}$$

Introducing the following dimensionless quantities

$$\tilde{r} = \frac{r}{u_*}, \quad \tilde{q} = \frac{q}{u_*}, \quad \tilde{y} = \frac{y}{\lambda}, \quad \tilde{z} = \frac{z}{h}, \quad \tilde{t} = \frac{tu_*}{h}, \quad \tilde{\bar{v}}_t = \frac{\bar{v}_t}{u_*h}, \quad \tilde{\nu} = \frac{\nu}{u_*h}$$

and

$$\tilde{\phi}(\tilde{y}, \tilde{z}) = \phi(y, z) / \left(\frac{u_*^2}{\lambda^2 h} \right) \quad (12)$$

the governing equation can be put in dimensionless form as

$$\left(\frac{\partial}{\partial \tilde{t}} - \tilde{\nu} \tilde{\nabla}^2 \right) \tilde{\nabla}^2 \tilde{r} = \tilde{\phi}(\tilde{y}, \tilde{z}) + \tilde{\bar{v}}_t \left(\frac{\partial^4 \tilde{r}}{\partial \tilde{z}^4} - 2 \frac{\partial^4 \tilde{r}}{\partial \tilde{y}^2 \partial \tilde{z}^2} + \frac{\partial^4 \tilde{r}}{\partial \tilde{y}^4} \right) \quad (13)$$

where the length λ of rough bed strip is assumed as same as flow height h . Under the steady and uniform flow conditions, equation (13) can be expressed as

$$(\tilde{\nu} + \tilde{\bar{v}}_t) \frac{\partial^4 \tilde{r}(\tilde{y}, \tilde{z})}{\partial \tilde{z}^4} + 2(\tilde{\nu} - \tilde{\bar{v}}_t) \frac{\partial^4 \tilde{r}(\tilde{y}, \tilde{z})}{\partial \tilde{y}^2 \partial \tilde{z}^2} + (\tilde{\nu} + \tilde{\bar{v}}_t) \frac{\partial^4 \tilde{r}(\tilde{y}, \tilde{z})}{\partial \tilde{y}^4} = -\tilde{\phi}(\tilde{y}, \tilde{z}). \quad (14)$$

Equation (14) is the governing equation for the vertical component $\tilde{r}(\tilde{y}, \tilde{z})$ of secondary current which includes both the generation and suppression of secondary current as well as effect of viscosity due to the mixing sediment particles in the flow domain. To solve equation (14) for $\tilde{r}(\tilde{y}, \tilde{z})$, boundary and other conditions are required. Since this study focuses on the cellular secondary currents and streamwise bed configurations, the boundary conditions are considered from the latest experimental observations and study by Wang and Cheng (2005) and Wang and Cheng (2006). In these experiments it is observed that vertical secondary flow velocity is absent in both the channel bottom and free surface due to the presence of boundaries. Also it has been observed that at every section along the lateral direction, the maximum value of vertical secondary flow velocity always occurs at the middle of the flow depth. Starting from zero velocity at the channel bottom, vertical secondary velocity gradually increases towards the middle of flow depth and then eventually decreases and becomes zero at the free surface. It is also found by Wang and Cheng (2006) that at the junction of smooth and rough bed strips, vertical velocity vanishes over the whole flow depth and transverse component of the secondary current exists. Considering these, the boundary conditions can be formulated as

$$\begin{aligned} \tilde{r}(\tilde{y}, \tilde{z}) \Big|_{\tilde{z}=0} &= 0, \quad \tilde{r}(\tilde{y}, \tilde{z}) \Big|_{\tilde{z}=1} = 0, \\ \tilde{r}(\tilde{y}, \tilde{z}) \Big|_{|\tilde{y}|=2m+1, \tilde{z}=1/2} &= \tilde{W}_{\max}, \quad \frac{\partial \tilde{r}}{\partial \tilde{z}} \Big|_{\tilde{z}=1/2} = 0, \end{aligned}$$

and

$$\tilde{r}(\tilde{y}, \tilde{z}) \Big|_{|\tilde{y}|=(2m+1)/2} = 0 \quad (15)$$

where $m = 0, 1, 2, 3, \dots$ and $\tilde{W}_{\max} = W_{\max}/u_*$ is the dimensionless maximum upwelling velocity Wang and Cheng (2006). In the formulation of equations (15), the bed configuration similar to Wang and Cheng (2006) is assumed and these conditions can be changed accordingly for other types of bed configurations with suitable length scales (flow height and length of rough bed strips) and co-ordinate system. It is important to mention here that equation (14) is a partial differential equation and one can solve it by using any standard numerical methods along with the specified boundary conditions in equation (15). But finding a complete analytical solution is very much challenging which is addressed in this study. The main motivation is to find an analytical solution which is easy for practical applications without any hard core numerical simulations or empirical assumptions. These analytical solutions not only provide hand free

solutions, but also improve our understanding towards the effects of included parameters of the physical process.

3. Analytical closed form solution

In most of the considered three dimensional turbulent flows, though the magnitude of the secondary component velocities is apparently less than 5% of the magnitude of primary flow velocity, but their effects on primary velocity, suspension distribution and settling velocity cannot be neglected (Guo 1998, Kundu and Ghoshal 2014). In the present study we focus on the generation of secondary currents by variation of bed roughness. These changes in bed configuration serve as effective bed disturbances. To compare with experiments, we assume the flow as combination of ‘base flow’ and a perturbation to the base flow due to the existence of secondary currents. This assumption is possible due to the fact that secondary flow is generally much weaker than the primary flow Wang and Cheng (2005) and secondary flow is generated gradually upon the base flow since the initiation of motion. Further it is found from the literatures that in wide open channels, among many causes for development of secondary flows, it also occurs due to perturbation in bed roughness. To emphasize the effect of bed disturbances, here we assume that the secondary flow is comprised of an idealized secondary flow and a modification to the bed configuration or bed effects. This type of assumption is already employed in some previous studies (Wang and Cheng 2005, Lu *et al* 2018). Therefore, to solve the definite problem in equation (14), it is assumed that $\tilde{r}(\tilde{y}, \tilde{z}) = \tilde{W}_1(\tilde{y}, \tilde{z}) + \lambda_* \tilde{W}_2(\tilde{y}, \tilde{z})$ where $\tilde{W}_1(\tilde{y}, \tilde{z})$ is the idealized secondary flow, $\tilde{W}_2(\tilde{y}, \tilde{z})$ is the quantity related to perturbation in the flow due to the bed configuration and λ_* is a parameter related to bed perturbation. In their study, Yang *et al* (2012) found that the gradients in the wall-tangential direction is much smaller than the gradient in the wall-normal direction. Equation (14) is satisfied by both the functions $\tilde{W}_1(\tilde{y}, \tilde{z})$ and $\tilde{W}_2(\tilde{y}, \tilde{z})$. Since near to bed, W_2 plays significant role than the other part, following the results of Yang *et al* (2012), it is further assumed that the wall-tangential gradient terms of W_2 are negligible. Therefore, the definite problem can be decomposed into two simple problems which are expressed below along with their boundary conditions as,

$$(I) \quad \begin{cases} A \frac{\partial^4 \tilde{W}_2(\tilde{z})}{\partial \tilde{z}^4} = -\tilde{\phi}(\tilde{y}, \tilde{z}) \\ \tilde{W}_2(\tilde{z}) \Big|_{\tilde{z}=0} = 0, \quad \tilde{W}_2(\tilde{z}) \Big|_{\tilde{z}=1} = 0, \quad \frac{\partial \tilde{W}_2}{\partial \tilde{z}} \Big|_{\tilde{z}=1/2} = 0, \\ \tilde{W}_2(\tilde{y}, \tilde{z}) \Big|_{|\tilde{y}|=(2m+1)/2} = 0 \end{cases} \quad (16)$$

and

$$(II) \quad \begin{cases} A \frac{\partial^4 \tilde{W}_1(\tilde{y}, \tilde{z})}{\partial \tilde{z}^4} + B \frac{\partial^4 \tilde{W}_1(\tilde{y}, \tilde{z})}{\partial \tilde{y}^2 \partial \tilde{z}^2} + A \frac{\partial^4 \tilde{W}_1(\tilde{y}, \tilde{z})}{\partial \tilde{y}^4} = 0 \\ \tilde{W}_1(\tilde{y}, \tilde{z}) \Big|_{\tilde{z}=0} = 0, \quad \tilde{W}_1(\tilde{y}, \tilde{z}) \Big|_{\tilde{z}=1} = 0, \quad \text{and} \quad \frac{\partial \tilde{W}_1}{\partial \tilde{z}} \Big|_{\tilde{z}=1/2} = 0, \\ \tilde{W}_1(\tilde{y}, \tilde{z}) \Big|_{|\tilde{y}|=(2m+1)/2} = 0 \end{cases} \quad (17)$$

where $m = 0, 1, 2, 3, \dots$, $A = \tilde{\nu} + \tilde{\nu}_t$ and $B = 2(\tilde{\nu} - \tilde{\nu}_t)$.

Integrating and applying the boundary conditions in equation (16), the solution \tilde{W}_2 is expressed as

$$\begin{aligned} \tilde{W}_2(\tilde{y}, \tilde{z}) = & -L \cos(\pi \tilde{y}) \left(\frac{\tilde{z}^4}{24} - \frac{\tilde{z}^5}{60} - \frac{\tilde{z}}{64} \right) + \frac{9}{40} L \cos(\pi \tilde{y}) \left(\frac{\tilde{z}^3}{6} - \frac{\tilde{z}}{8} \right) \\ & + FL \cos(\pi \tilde{y}) \left(\frac{\tilde{z}^2}{2} - \frac{\tilde{z}}{2} \right) \end{aligned} \quad (18)$$

where $L = \frac{\alpha_0 \alpha \pi^3}{A}$ and F is a parameter determined from the experimental observation (For detailed step-by-step solution, see [appendix](#)). For the solution of the sub problem (II), the method of separation of variable is applied. Proceeding the calculation (see [appendix](#) for details) the solution $\tilde{W}_1(\tilde{y}, \tilde{z})$ is expressed as

$$\tilde{W}_1(\tilde{y}, \tilde{z}) = C_1 \frac{\sin(\pi \tilde{z})}{\sin\{\chi_1(\frac{2m+1}{2})\}} \sin\left\{\left(\frac{2m+1}{2} - |\tilde{y}|\right)\chi_1\right\} \quad (19)$$

where $C_1 = \lambda_* L \left(\frac{F}{8} + \frac{7}{1920}\right) - \tilde{W}_{\max}$. Therefore the solution $\tilde{r}(\tilde{y}, \tilde{z})$ can be expressed in the following as

$$\begin{aligned} \tilde{r}(\tilde{y}, \tilde{z}) = & \left[\lambda_* L \left(\frac{F}{8} + \frac{7}{1920} \right) - \tilde{W}_{\max} \right] \frac{\sin(\pi \tilde{z})}{\sin\{\chi_1(\frac{2m+1}{2})\}} \\ & \sin\left\{\left(\frac{2m+1}{2} - |\tilde{y}|\right)\chi_1\right\} - \lambda_* L \cos(\pi \tilde{y}) \\ & \times \left[\left(\frac{\tilde{z}^4}{24} - \frac{\tilde{z}^5}{60} - \frac{\tilde{z}}{64} \right) - \frac{9}{40} \left(\frac{\tilde{z}^3}{6} - \frac{\tilde{z}}{8} \right) - F \left(\frac{\tilde{z}^2}{2} - \frac{\tilde{z}}{2} \right) \right]. \end{aligned} \quad (20)$$

The transverse component of secondary flow $\tilde{q}(\tilde{y}, \tilde{z})$ can be obtained from the continuity equation equation (1) after the integration and using the condition $\tilde{q}(\tilde{y} = \pm m) = 0$ where $m = 0, 1, 2, 3, \dots$ as

$$\begin{aligned} \tilde{q}(\tilde{y}, \tilde{z}) = & (-1)^N \left[\lambda_* L \left(\frac{F}{8} + \frac{7}{1920} \right) - \tilde{W}_{\max} \right] \frac{\pi \cos(\pi \tilde{z})}{\chi_1 \sin\{\chi_1(\frac{2m+1}{2})\}} \\ & \times \left[\cos\left\{\chi_1\left(\frac{2m+1}{2} - |\tilde{y}|\right)\right\} - \cos\left\{\frac{\chi_1}{2}\right\} \right] + \left(\frac{\lambda_* L}{\pi}\right) \sin(\pi \tilde{y}) \\ & \times \left[\left(\frac{\tilde{z}^3}{6} - \frac{\tilde{z}^4}{12} - \frac{1}{64} \right) - \frac{9}{40} \left(\frac{\tilde{z}^2}{2} - \frac{1}{8} \right) - F \left(\tilde{z} - \frac{1}{2} \right) \right] \end{aligned} \quad (21)$$

with

$$N = \begin{cases} 0 & \text{when } \tilde{y} < 0, \\ 1 & \text{when } \tilde{y} > 0. \end{cases} \quad (22)$$

It can be seen from equations (20) and (21) that it contains the unknown F . To find the value of it, further the condition $\tilde{q} = \tilde{W}_{\max}$ at $\tilde{z} = 1$ and $\tilde{y} = -1/2$ is applied from experiments of Wang and Cheng (2006). This gives the value of the parameter F as

$$F = \frac{(1 + G)\tilde{W}_{\max} - L\lambda_* \left(\frac{1}{60\pi} + \frac{7G}{1920} \right)}{\frac{L\lambda_*}{2\pi} + \frac{LG\lambda_*}{8}} \quad \text{where } G = \frac{\pi [\cos(\chi_1/2) - 1]}{\chi_1 \sin(\chi_1/2)}. \quad (23)$$

Equations (20) and (21) represent the proposed new analytical models for secondary velocity components in straight rectangular wide open channel flows. It can be observed that in both

these equations, velocity components are made dimensionless using u_* . Since the magnitude of the vertical and transverse flow velocities are less (1%–2%) compared to the primary flow velocity, it is more reasonable to make dimensionless with its maximum values W_{\max} . In the experiment by Wang and Cheng (2006), it has been observed that $W_{\max} = 0.02 U_m$ where U_m is the mean value of primary flow velocity at the central section. The mean velocity U_m is computed from the below formula as

$$(1 - \tilde{z}_0)U_m = \int_{\tilde{z}_0}^1 \frac{u_*}{\kappa} \ln\left(\frac{\tilde{z}}{\tilde{z}_0}\right) d\tilde{z} = \frac{u_*(1 - \tilde{z}_0)}{\kappa} \left[-1 - \frac{\ln \tilde{z}_0}{1 - \tilde{z}_0}\right] \quad (24)$$

where $\tilde{z}_0 = z_0/h$ and z_0 denotes the zero primary velocity level. Equations (20) and (21) give the most general solution for the vertical and transverse secondary flow velocities till now. The parameter A present in the model includes the effect of fluid viscosity which is generally neglected. The next section, describes the validation of these proposed analytical models with existing experimental data and also discusses the comparison results with existing models.

4. Validation with laboratory flume data

In this section, computed results of the vertical and transverse components of secondary flow velocities from equations (20) and (21) respectively are validated with laboratory flume data. Apart from it, these models are also compared with the existing models proposed by Kotsovinos (1988) and Wang and Cheng (2006) to get a better idea about the accuracy of these models. For the validation purpose, experimental data of Gessner and Emery (1981), Wang and Cheng (2006), Proust and Nikora (2020) and Soualmia *et al* (2008) are considered in this study for a wide variety of flows. More precisely, to test the validity of the proposed model in wide rectangular open channel flow, experimental data of Wang and Cheng (2006) is considered; for the validity in compound channel flow, experimental data of Proust and Nikora (2020) is chosen; and for the applicability in closed duct flow, experimental data of Gessner and Emery (1981) and simulated data of Soualmia *et al* (2008) are considered.

In figures 5 and 6 contour lines of secondary flow velocities in the yz cross sectional plane are presented for these two proposed models together with the models of Wang and Cheng (2006). Models of Wang and Cheng (2006) are plotted in the same figure for comparison purposes. In both the figures, the vertical velocity component $r(\tilde{y}, \tilde{z})$ and the lateral velocity component $q(\tilde{y}, \tilde{z})$ both are made dimensionless using W_{\max} , maximum value of the vertical velocity. This W_{\max} is computed as discussed earlier. Shear velocity is calculated from $u_* = \sqrt{gJh}$. The values of parameters are kept as $\tilde{\nu}_t = 0.0547$, $u_* = 0.03 \text{ m s}^{-1}$, $W_{\max} = 0.0095 \text{ m s}^{-1}$, $J = 0.0012$, $\lambda_* = 0.1$, $\alpha = 0.2$ (obtained from equation (9) after fitting the Reynolds shear stress model with observational data), $F = -0.0577$ (computed from equation (23)) and $\tilde{z}_0 = 6 \times 10^{-4}$ for figure 5 and $\tilde{\nu}_t = 0.0547$, $u_* = 0.03 \text{ m s}^{-1}$, $W_{\max} = 0.0095 \text{ m s}^{-1}$, $J = 0.0012$, $\lambda_* = -0.01$, $\alpha = 0.2$, $F = 0.0343$ and $\tilde{z}_0 = 2 \times 10^{-5}$ for figure 6. From both the figures it can be seen that contour lines from the proposed model agree well with the models of Wang and Cheng (2006). The advantage of the proposed model is that it contains the secondary current parameter α and fluid viscosity which enhances the applicability of the proposed models to other type of fluids. Apart from this, proposed models are derived mathematically rather than assuming them empirically, unlike most of the previous studies done. Apart from these, to validate the results for a large interval in wide open channels, contours of r/W_{\max} and q/W_{\max} are plotted in figures 7 and 8 respectively for the interval $[-3, 3]$ along with the model of (Wang and Cheng 2006). It can be concluded after comparing the plots of two models that results of the proposed model are similar and comparable with the existing model.

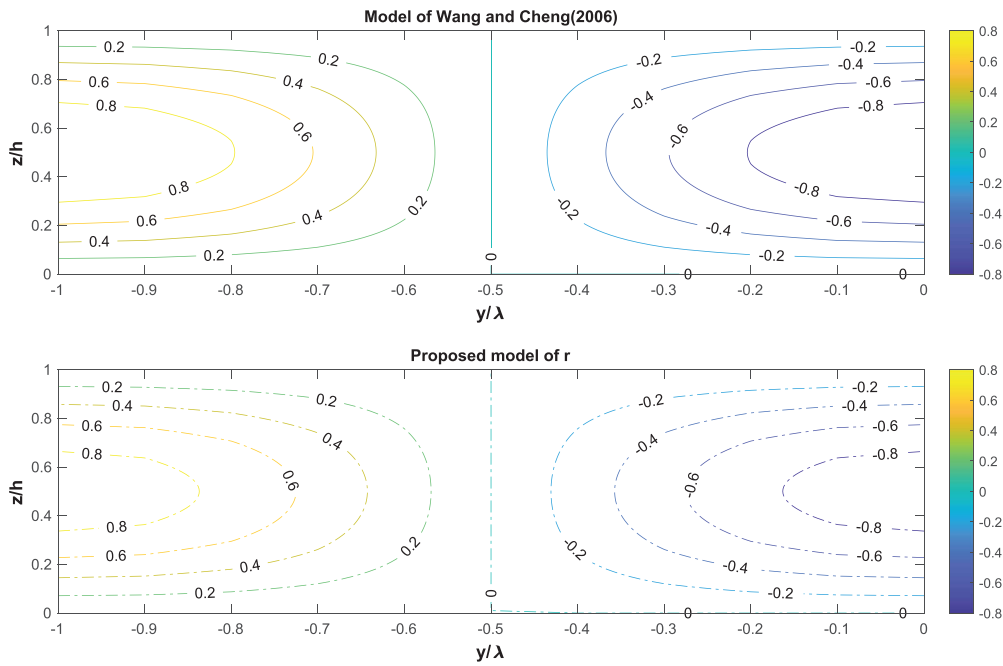


Figure 5. Comparison of contours of $r(\tilde{y}, \tilde{z})/W_{\max}$ between model of Wang and Cheng (2006) and proposed model (equation (20)). Flow conditions are $\tilde{v}_t = 0.06$, $u_* = 0.03 \text{ m s}^{-1}$, $W_{\max} = 0.0095 \text{ m s}^{-1}$, $J = 0.0012$, $\alpha = 0.2$, $\lambda_* = 0.1$, $\tilde{z}_0 = 6 \times 10^{-4}$.

Figures 9 and 10 show the validity of the proposed models of secondary current with the experimental data of Wang and Cheng (2006). In these figures, dimensionless vertical and transverse velocity components are plotted against the vertical height z/h at different channel sections $y/\lambda = 0.0, -0.1, -0.2, \dots, -1.0$ along spanwise direction. Models of Wang and Cheng (2006) and Kotsovinos (1988) (both are same) are also plotted in the figure for comparison purposes. Flow conditions are taken from the experiments of Wang and Cheng (2006) which are as follows: $B = 0.6 \text{ m}$, $h = 0.0075 \text{ m}$, $J = 0.0012$, $u_* = 0.03 \text{ m s}^{-1}$ and W_{\max} is computed as mentioned earlier using the formula in equation (24). Other values of parameters are kept fixed as mentioned in figures 5 and 6. From figure 9 it can be seen that, at $y/\lambda = -0.5$ (smooth and rough strip interface) computed vertical flow velocity becomes almost zero over the full water depth which agrees well with experimental data. The zero vertical velocity occurs due to sudden change in bed roughness where the vertical secondary current is almost negligible. In the figure, it is also observed that positive and negative vertical velocities in regions $-1.0 \leq y/h < -0.5$ and $-0.5 < y/h \leq 0$ respectively are well explained by the model. The change in magnitude of the vertical flow velocity occurs due to change in direction (upflow and downflow) of the secondary current. Furthermore, it can be seen in figure 9 that when $y/\lambda = 0$ and -1 , predicted values of vertical secondary velocity from the model deviate from the experimental data. This can be explained as follows. Models are developed by expressing the transverse Reynolds shear stress in terms of secondary velocity gradients $\frac{\partial r}{\partial y}$ and $\frac{\partial q}{\partial z}$ using eddy viscosity concept after following Ikeda (1981) and Hinze (1975). Naot and Rodi (1982) pointed out that turbulence closure models based on the eddy viscosity concept cannot fully reproduce the turbulence-induced secondary currents. Along these channel sections vertical secondary current is acting completely along the upward or downward directions and relatively stronger

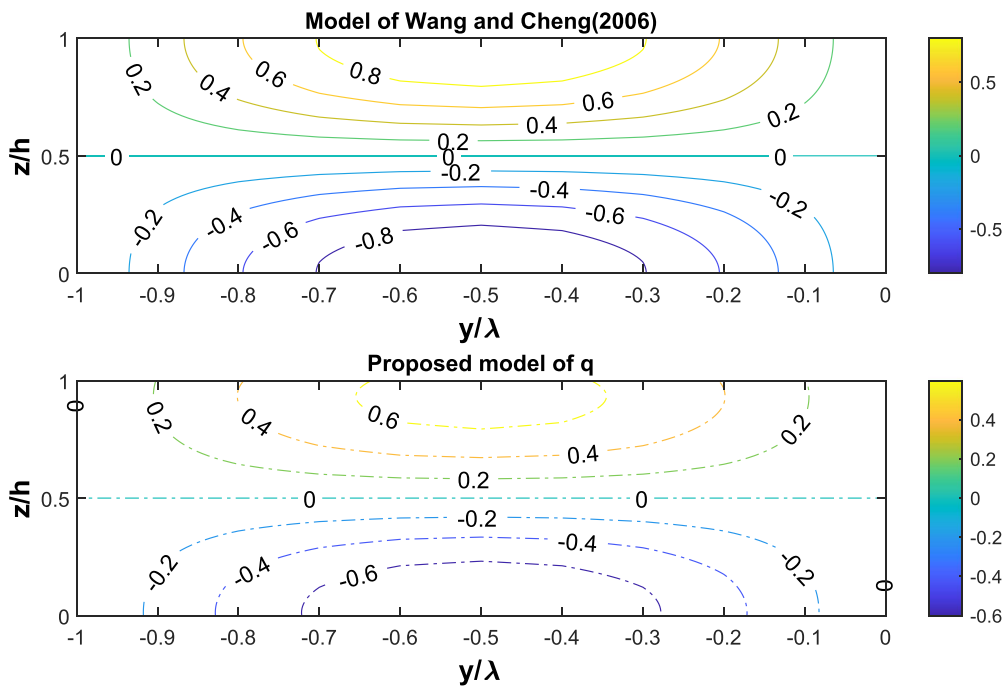


Figure 6. Comparison of contours of $q(\tilde{y}, \tilde{z})/W_{\max}$ between model of Wang and Cheng (2006) and proposed model (equation (21)). Flow conditions are $\tilde{v}_t = 0.06$, $u_* = 0.03 \text{ m s}^{-1}$, $W_{\max} = 0.0095 \text{ m s}^{-1}$, $J = 0.0012$, $\alpha = 0.2$, $\lambda_* = -0.01$, $\tilde{z}_0 = 2 \times 10^{-5}$.

than other parts of the channels, as a result predicted model values deviate at these channel sections. Similarly, in figure 10 it can be observed that at $y/\lambda = 0.0$ (central section) and -1.0 (mid point of smooth strips), transverse velocity is zero. At these sections, secondary velocity is directed along vertical directions. It can also be observed that predicted model value deviates from the data when $y/\lambda = -0.5$. This is due to the fact that at this channel section, transverse secondary current is completely acting along the transverse direction and relatively stronger than other part of the channel which results the deviation from the data. Though the discrepancy occurs but the proposed model gives better approximation than existing model. It is to be noted that the turbulence closure models are generally expressed through eddy viscosity which is also used in here. The model prediction can be improved if other forms of turbulence closure are assumed. This may lead to numerical solution of the model which is cost effective and computationally complex and does not match with the objective in this study. Though interested readers can improve the results. It is clear from the validation results in these two figures that proposed model predicts data well in general and comparable to the previous model of Wang and Cheng (2006).

The validity of the proposed model for compound open channel flows is presented in figures 11 and 12. In these figures, recent experimental data of Proust and Nikora (2020) are considered. The experiment was conducted in an 18 m long and 3 m wide compound channel with bed slope J as 1.1×10^{-3} . The cross section is comprised of a 1 m wide main channel which is flanked by two 1 m wide flat rough surface symmetrically. Among all data sets, the uniform flow data set (case 8) are considered in this study. Figure 11 shows the validation for

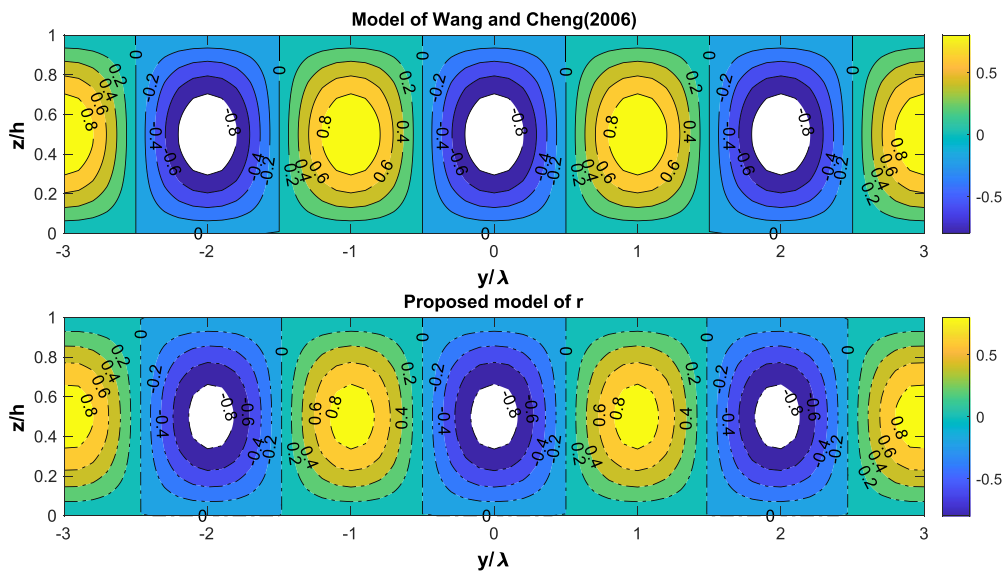


Figure 7. Contour of $r(\bar{y}, \bar{z})/W_{\max}$ for model of Wang and Cheng (2006) and proposed model (equation (20)) over the interval $[-3, 3]$.

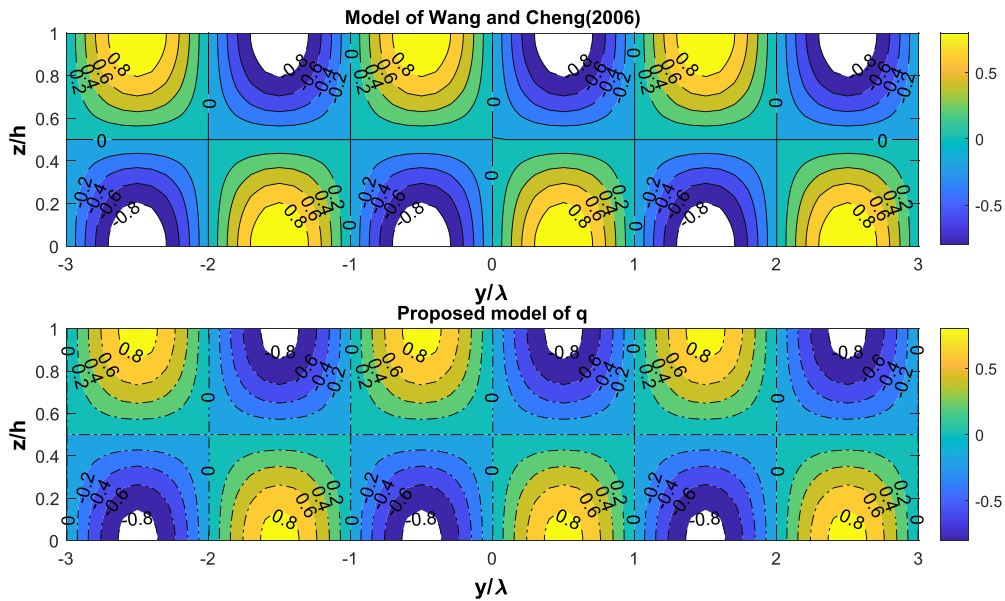


Figure 8. Contour of $q(\bar{y}, \bar{z})/W_{\max}$ for model of Wang and Cheng (2006) and proposed model (equation (21)) over the interval $[-3, 3]$.

vertical velocity and figure 12 for the transverse velocity as a total of seven different sections along transverse direction. In both the figures, secondary velocities are made dimensionless using the shear velocity u_* which is computed using the formulas \sqrt{gJh} . The flow height h is taken the height of the flow at the main channel. Values of all other parameters are taken from

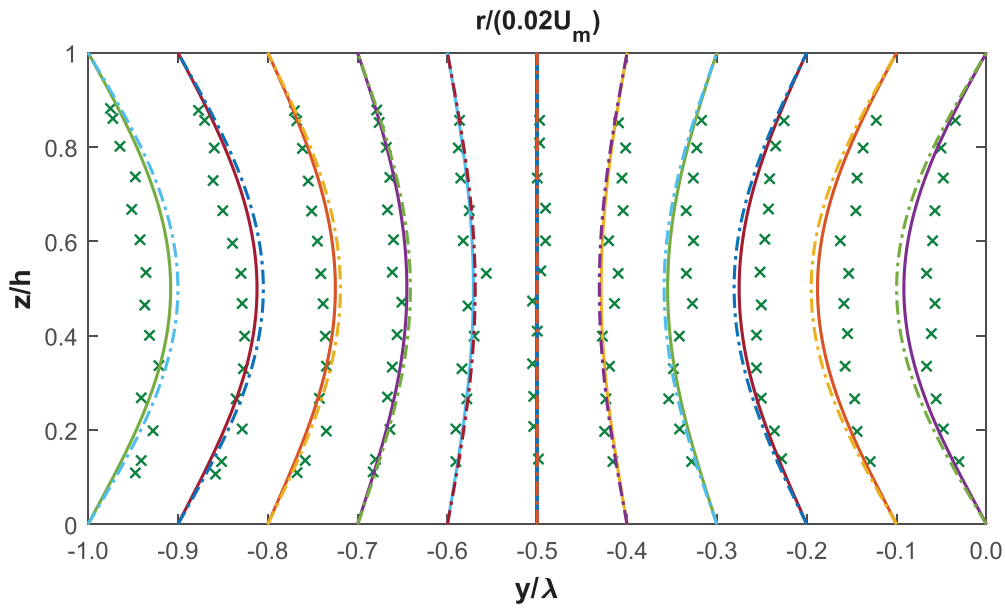


Figure 9. Validation and comparison of the proposed model (equation (20)) of $r(\bar{y}, \bar{z})/W_{\max}$ with experimental data of Wang and Cheng (2006) and existing empirical model of Wang and Cheng (2006). Continuous lines (-) denote proposed model, dash dotted lines (-.-) denote model of Wang and Cheng (2006) and crosses (\times) denote data points. Flow conditions are $B = 0.6$ m, $h = 0.0075$ m, $J = 0.0012$, $u_* = 0.03$ m s $^{-1}$ and $W_{\max} = 0.0095$ m s $^{-1}$, $\alpha = 0.2$, $\lambda_* = 0.1$, $\bar{z}_0 = 6 \times 10^{-4}$.

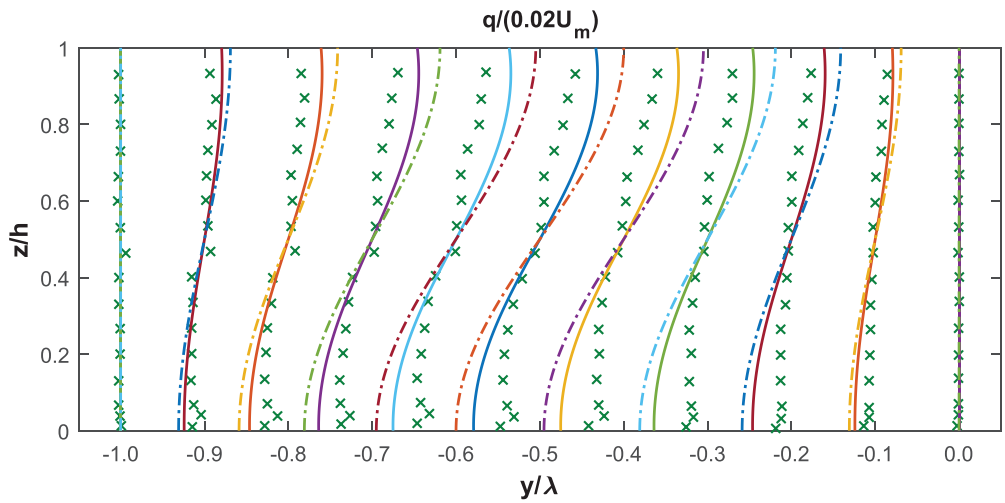


Figure 10. Validation and comparison of the proposed model (equation (21)) of $q(\bar{y}, \bar{z})/W_{\max}$ with experimental data of Wang and Cheng (2006) and existing empirical model of Wang and Cheng (2006). Continuous lines (-) denote proposed model, dash dotted lines (-.-) denote model of Wang and Cheng (2006) and crosses (\times) denote data points. Flow conditions are $B = 0.6$ m, $h = 0.0075$ m, $J = 0.0012$, $u_* = 0.03$ m s $^{-1}$ and $W_{\max} = 0.0095$ m s $^{-1}$, $\alpha = 0.2$, $\lambda_* = -0.01$, $\bar{z}_0 = 2 \times 10^{-5}$.

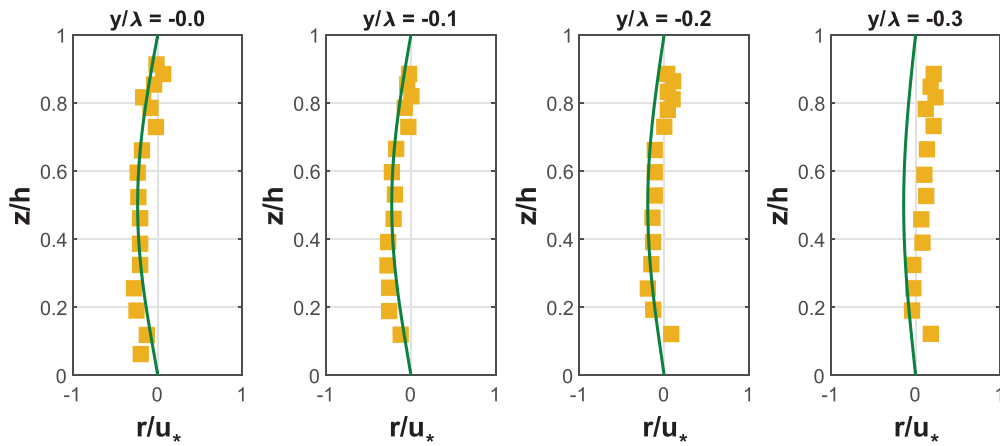


Figure 11. Validation of the proposed model (equation (20)) for compound channel of $r(\tilde{y}, \tilde{z})/u_*$ with experimental data of Proust and Nikora (2020). Continuous lines (-) denote proposed model and squares (■) denote data points. Flow conditions are $B = 3$ m, $h = 0.147$ m, $J = 0.0011$, $u_* = 0.0399$ m s⁻¹.

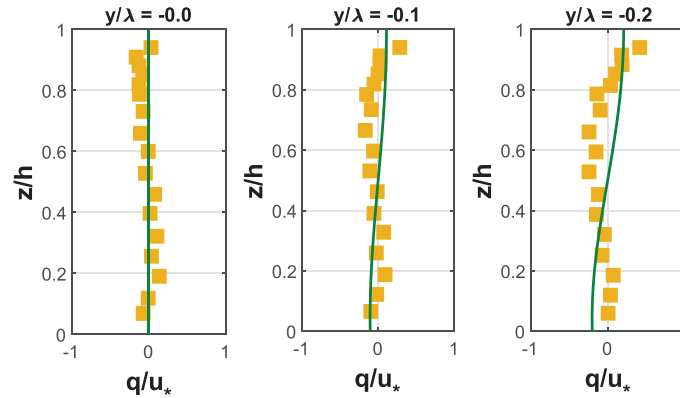


Figure 12. Validation of the proposed model (equation (21)) for compound channel of $q(\tilde{y}, \tilde{z})/u_*$ with experimental data of Proust and Nikora (2020). Continuous lines (-) denote proposed model and squares (■) denote data points. Flow conditions are $B = 3$ m, $h = 0.147$ m, $J = 0.0011$, $u_* = 0.0399$ m s⁻¹, $W_{\max} = 0.0142$ m s⁻¹, $\tilde{z}_0 = 3.1 \times 10^{-4}$.

the experimental data mentioned in Proust and Nikora (2020). From both the figures, it can be seen that both the proposed models predict the data well in this case also.

Figure 13 shows the validity of the transverse velocity component $q(\tilde{y}, \tilde{z})$ along lateral direction with the experimental data of Proust and Nikora (2020) at vertical height $z/h = 0.94$. The data in the main channel is considered here for the validation purpose. The values of parameters are kept as $\alpha = 0.9$ for computation from the proposed model. It can be seen from the figure, that in general proposed model predicts data well almost over the whole cross section but there is a slight discrepancy between observed and computed values around the point $y/h = -0.45$. In the region $-0.45 \leq y/h \leq -0.4$, transverse velocity tends to be zero which can be explained as follows: near the section at $y/h = -0.45$, the junction of the compound channel appears

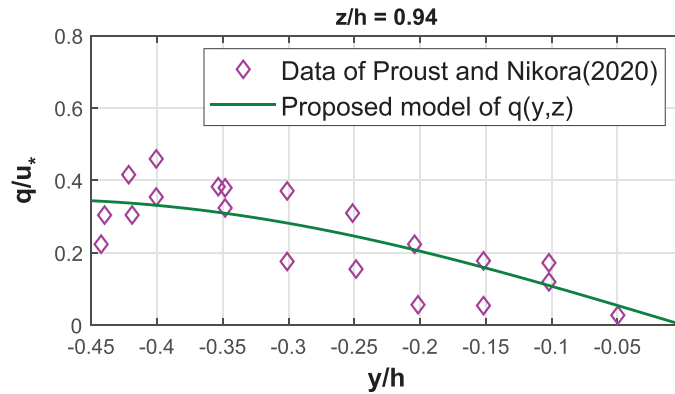


Figure 13. Validation of the transverse distribution of $q(\bar{y}, \bar{z})/u_*$ at $z/h = 0.94$ with experimental data of Proust and Nikora (2020) for uniform flow condition.

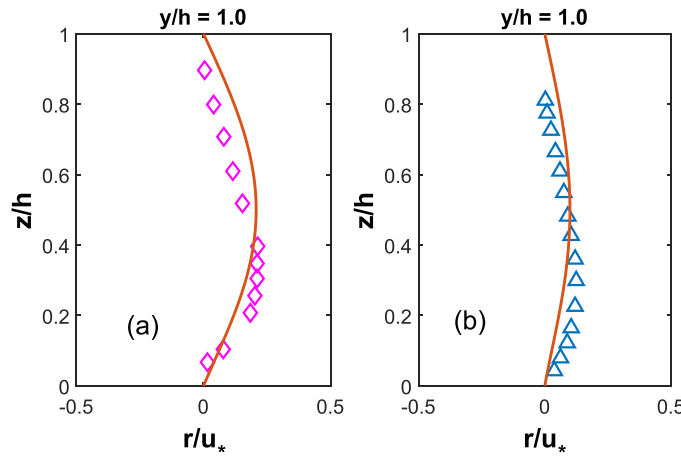


Figure 14. Validation of the proposed model (equation (20)) of $r(\bar{y}, \bar{z})/u_*$ in duct flow with experimental data of (a) Gessner and Emery (1981) and (b) Soualmia *et al* (2008). Continuous lines (-) denote proposed model, open diamonds (\diamond) denote data of Gessner and Emery (1981) and triangles (Δ) denote data points of Soualmia *et al* (2008).

where there is a sudden change in flow depth. The vertical deviation at the point $y/h = -0.45$ creates a separation line between two circular secondary cells of different dimensions and along which only vertical velocity component exists (as observed in the experiment of Proust and Nikora (2020)). As a result, transverse component of secondary velocity appears to be zero.

Finally, the validation of the proposed model of vertical velocity for closed duct flow is presented in figure 14 with experimental data of Gessner and Emery (1981) and simulated data of Soualmia *et al* (2008) at the channel central section. In both the figures the vertical velocity is made dimensionless using the mean flow U_m . The values of the parameters are kept as: $W_{\max} = 0.0056 \text{ m s}^{-1}$, $\lambda_* = 0.1$, $\alpha = 0.2$, and $\bar{z}_0 = 6 \times 10^{-3}$ for data of Gessner and Emery (1981) and $W_{\max} = 0.003 \text{ m s}^{-1}$, $\lambda_* = 0.1$, $\alpha = 0.2$, and $\bar{z}_0 = 6 \times 10^{-2}$ for data of Soualmia

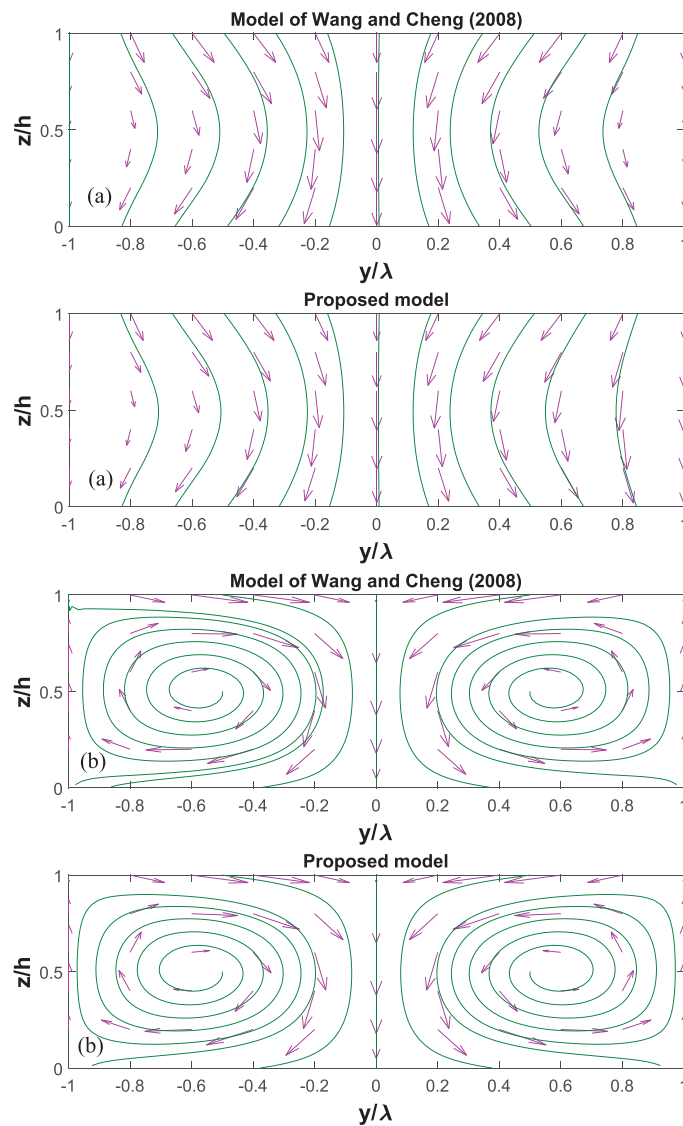


Figure 15. Comparison of ω -streamlines from equation (28) with existing empirical model of Wang and Cheng (2008) for (a) $W_{\max}/\omega_0 = 0.5$ and (b) $W_{\max}/\omega_0 = 5$.

et al (2008). Both the comparison results suggest that proposed model for vertical component of secondary current can be applied for duct flows also.

5. Discussions

In this section, applications of the proposed models of vertical and lateral components of secondary current on the settling velocity vector is discussed. New modified models of settling velocity vector incorporating the improved secondary velocity models are also suggested.

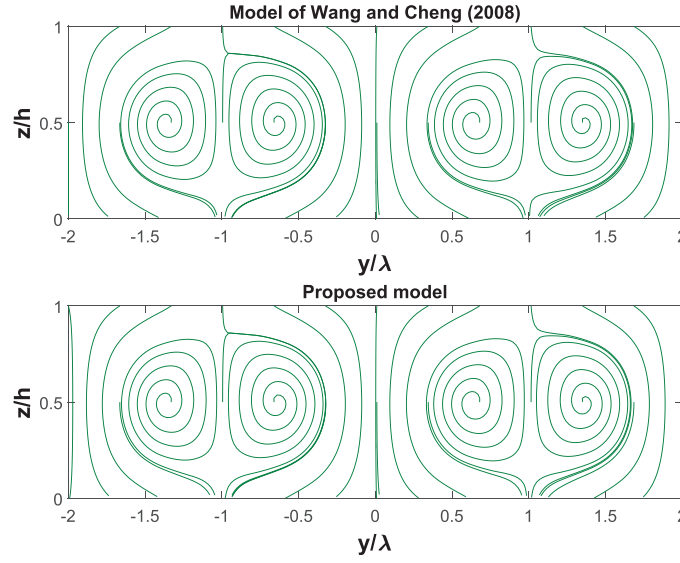


Figure 16. Comparison of retention zones for sediment particles in the cross-sectional yz -plane for $W_{\max}/\omega_0 = 2.5$ with model of Wang and Cheng (2008).

5.1. Effect of secondary current on settling velocity vector

Wang and Cheng (2008) investigated the effect of secondary currents on the structures of streamlines of the settling velocity vector. Under negligible flow acceleration and uniform relative velocity between sediment particle and ambient fluid, settling velocity vector $\vec{\omega}_s$ in sediment-mixed fluid is expressed by Wang and Cheng (2008) as

$$\vec{\omega}_s = \vec{\omega}_0 + \vec{V}_{\text{lag}} \quad (25)$$

where $\vec{\omega}_0$ is settling velocity vector in still fluid and \vec{V}_{lag} is the velocity vector corresponding to the secondary flows. The settling velocity vector $\vec{\omega}_0$ is expressed as

$$\vec{\omega}_0 = -\omega_0 \hat{k} \quad (26)$$

where ω_0 is single particle settling velocity in still clear water and \hat{k} is the unit vector along the vertical z direction. As mentioned earlier, secondary currents in wide open channels can be generated due to several factors. Since in this study generation of secondary current is considered through the variation of bed roughness, the velocity vector \vec{V}_{lag} is expressed according to Wang and Cheng (2008) as

$$\vec{V}_{\text{lag}} = q(\tilde{y}, \tilde{z})\hat{j} + r(\tilde{y}, \tilde{z})\hat{k}. \quad (27)$$

Equation (27) indicates that the velocity vector due to secondary flow can be affected by both the secondary flow components and thus applicable in whole yz cross sectional plane. Substituting equations (26) and (27) into equation (25) and using equations (20) and (21) the settling velocity vector is expressed as

$$\begin{aligned}
\frac{\vec{\omega}_s}{\omega_0} &= \left\{ \frac{q(\tilde{y}, \tilde{z})}{\omega_0} \right\} \hat{j} + \left\{ \frac{r(\tilde{y}, \tilde{z})}{\omega_0} - 1 \right\} \hat{k} = \left(\frac{u_*}{\omega_0} \right) \\
&\times \left\{ (-1)^N C_1 \frac{\pi \cos(\pi \tilde{z})}{\chi_1 \sin\{\chi_1 (\frac{2m+1}{2})\}} \left[\cos\left\{ \chi_1 \left(\frac{2m+1}{2} - |\tilde{y}| \right) \right\} - \cos(\chi_1/2) \right] \right. \\
&+ \left. \left(\frac{\lambda_* L}{\pi} \right) \sin(\pi \tilde{y}) \left[\left(\frac{\tilde{z}^3}{6} - \frac{\tilde{z}^4}{12} - \frac{1}{64} \right) - \frac{9}{40} \left(\frac{\tilde{z}^2}{2} - \frac{1}{8} \right) - F\left(\tilde{z} - \frac{1}{2}\right) \right] \right\} \hat{j} \\
&+ \left(\frac{u_*}{\omega_0} \right) \left\{ \left[\lambda_* L \left(\frac{F}{8} + \frac{7}{1920} \right) - \tilde{W}_{\max} \right] \frac{\sin(\pi \tilde{z})}{\sin\{\chi_1 (\frac{2m+1}{2})\}} \right. \\
&\times \sin\left\{ \left(\frac{2m+1}{2} - |\tilde{y}| \right) \chi_1 \right\} - \lambda_* L \cos(\pi \tilde{y}) \\
&\times \left. \left[\left(\frac{\tilde{z}^4}{24} - \frac{\tilde{z}^5}{60} - \frac{\tilde{z}}{64} \right) - \frac{9}{40} \left(\frac{\tilde{z}^3}{6} - \frac{\tilde{z}}{8} \right) - F\left(\frac{\tilde{z}^2}{2} - \frac{\tilde{z}}{2}\right) \right] - 1 \right\} \hat{k}. \quad (28)
\end{aligned}$$

Equation (28) shows the variation of the settling velocity variation in the cross-sectional yz -plane including its directions as well as magnitude. It can be observed from the equation that the streamlines of settling velocity depend on several factor such as maximum magnitude of the secondary flow velocity, dip correction parameter α , viscosity of the fluid and eddy viscosity. This proposed model of the hindered settling velocity in equation (28), is more general than the previous model proposed by Wang and Cheng (2008). Due to inclusion of these aforementioned factors, this equation is more realistic and appropriate for practical applications. For the validation purpose, the proposed model is compared with the model of Wang and Cheng (2008) and the result is shown in figure 15 for two different choices of the ratio W_{\max}/ω_0 . In the figure the streamlines of $\vec{\omega}_s$ in yz cross sectional plane is plotted along with the vector line segments with directions. Two totally different sceneries are observed which corresponds to $W_{\max}/\omega_0 < 1$ (In figure 15(a)) and $W_{\max}/\omega_0 > 1$ (In figure 15(b)). The values of other parameters for both the cases are kept as $\alpha = 0.2$, $\lambda_* = 0.1$, $W_{\max} = 0.0095 \text{ m s}^{-1}$ and $u_* = \sqrt{gJh} = 0.0297 \text{ m s}^{-1}$, $\tilde{z}_0 = 6 \times 10^{-6}$. It can be observed that when $W_{\max}/\omega_0 < 1$ all streamlines are open and directed toward the channel bed; whereas for $W_{\max}/\omega_0 > 1$, closed streamlines are obtained (except for $y/h = 0$) and are oriented in a cellular fashion. From both the figures it can be seen that proposed model gives good agreement with the model of Wang and Cheng (2008). Apart from it, in figure 16 the retention zones (the zone where sediment particles are trapped) are plotted from the proposed model together with the model of Wang and Cheng (2008) for $W_{\max}/\omega_0 = 2.5$ for comparison purposes. It can be concluded after comparing both the figures that proposed model gives comparable and accurate results for the prediction of retention zones. All these results show that the proposed model can be used as an efficient alternative model for predicting hindered settling velocity vector in the yz -cross sectional plane. Apart from this, since the present study also considered the effect of kinematic viscosity of the fluid as well as the eddy viscosity closure, this model can further be applied for other kinds of fluid.

6. Concluding remarks

This study proposes effective mathematical models of vertical and transverse secondary flow velocities in steady and uniform turbulent flows through straight open rectangular channels, compound rectangular channels and closed ducts. Most of the previous studies proposed and employed empirical models for secondary flow velocities using boundary conditions; whereas

in the present study, the general governing equation is first developed starting from the continuity and the Reynolds averaged Navier–Stokes equation including the effects of fluid viscosity. The governing equation is solved using suitable turbulence closures and appropriate and realistic boundary conditions. The novelty of the work lies in the consideration of viscous effect in the model, proposition of a new single Reynolds shear stress model for entire cross-section and the new analytical solution methodology and on the broad applicability. In the literature, most of the studies and methodologies were focused about the flow conditions rather than the bed configuration and proposed the empirically. This study considers fluid property as well as bed property together. The original mathematical equation is divided into two separate equations using the concept of linear approximation and emphasizing the bed perturbation effect. The obtained models are fully analytical in nature, contain effects of the fluid viscosity, eddy viscosity of turbulence and depend on the direction of secondary flow velocities and therefore more appropriate for practical use. Proposed models are validated using experimental data for open channel flows, compound channel flows and duct flows and also compared with existing empirical models to justify the effectiveness. From the validation and comparison results, it is found that proposed model can predict velocity data better than previous models in all mentioned channels. Apart from this, it is found that proposed models can also be applied to find velocities along transverse direction of channels. The findings of this study are further applied to investigate the effects of secondary currents on the hindered settling velocity vector in an entire cross-sectional plane. New effective alternative models for settling velocity vector is proposed. Further, it is found that secondary current significantly modifies the streamlines of settling particles and on the other hand, stream-wise Reynolds shear stress distributions deviate from its traditional linear model when secondary currents exist in the flow domain. The obtained results are well consistent with previous findings. The models of these study can further be applied to find boundary shear stress distributions, free surface flow velocity structures and to investigate one and two dimensional mean primary velocity distributions in the flow domain. Further, the study can be extended and improved using other types of turbulence closure models with numerical simulations.

Acknowledgment

Authors are very much thankful to Dr Koeli Ghoshal, Associate Professor of Dept. of Mathematics, IIT Kharagpur, India for her continuous support, discussions and corrections in the paper.

Conflict of interest

The authors declare that they have no conflict of interest.

Funding

There is no funding source.

Appendix

A.1. Derivation of eddy viscosity model

The eddy viscosity is generally expressed by relating it to the Reynolds shear stress as Yalin (1977)

$$-\overline{p'r'} = \nu_t \left(\frac{\partial p}{\partial z} + \frac{\partial r}{\partial x} \right). \tag{29}$$

Under such complex flow, the Reynolds shear stress deviates from the linear profile (Yang *et al* 2004). Yang *et al* (2004) proposed the following model for such flows as

$$-\frac{\overline{p'r'}}{u_*^2} = \frac{\tau_t}{\rho u_*^2} = 1 - \frac{z}{h} - \alpha \frac{z}{h}. \tag{30}$$

The primary flow velocity is considered as the total-dip-modified-log-wake law (TDMLWL) as it gives more effective result than the log-law and other laws in literature Kundu and Ghoshal (2012). The TDMLWL is expressed as

$$\frac{p}{u_*} = \frac{1}{\kappa} \ln \left(\frac{z}{z_0} \right) + \frac{\alpha}{\kappa} \ln \left(1 - \frac{z}{h} \right) + \frac{2\Pi}{\kappa} \left[3 \left(\frac{z}{h} \right)^2 - 2 \left(\frac{z}{h} \right)^3 \right] - \frac{4\alpha\Pi}{\kappa} \left(\frac{z}{h} \right)^3 \tag{31}$$

where z_0 is the zero velocity depth, Π is Coles' wake parameter (treated as constant. The value is considered as 0.19 as suggested by Coleman (1981) for such flows) and α is the dip-correction parameter. Substituting equations (30) and (31) into equation (29), the modified eddy viscosity model for uniform flow is obtained as

$$\frac{\nu_t}{u_* h} = \kappa \left(1 - \frac{z}{h} \right) \left[\frac{h}{z} + 12\Pi \frac{z}{h} \left(1 - \frac{z}{h} \right) \right]^{-1}. \tag{32}$$

Equation (32) was first suggested by Kundu and Ghoshal (2012) for studying the effect of secondary flow on primary flow velocity and is employed here for such complex flow. Simultaneously, the depth averaged model of eddy viscosity is obtained as

$$\bar{\nu}_t = \frac{1}{h} \int_0^h \nu_t dz = \kappa u_* h \int_0^1 \frac{\tilde{z}(1-\tilde{z})}{1+12\Pi\tilde{z}^2(1-\tilde{z})} d\tilde{z}. \tag{33}$$

A.2. Detailed solutions

A.2.1. Detailed solution of sub-problem I. In this subsection the detailed solution of sub-problem (I) is explained. We consider the equation along with the boundary conditions such as,

$$\begin{aligned} A \frac{\partial^4 \tilde{W}_2(\tilde{y}, \tilde{z})}{\partial \tilde{z}^4} &= -\tilde{\phi}(\tilde{y}, \tilde{z}) \\ \tilde{W}_2(\tilde{z} = 0) &= 0, \quad \tilde{W}_2(\tilde{z} = 1) = 0, \quad \frac{\partial \tilde{W}_2}{\partial \tilde{z}} \Big|_{\tilde{z}=1/2} = 0, \\ \tilde{W}_2(|\tilde{y}| = (2m+1)/2) &= 0. \end{aligned} \tag{34}$$

After integrating equation (34) we get,

$$\tilde{W}_2(\tilde{y}, \tilde{z}) = -L \cos(\pi\tilde{y}) \left[\frac{\tilde{z}^4}{24} - \frac{\tilde{z}^5}{60} \right] + \frac{\tilde{z}^3}{6} f_1(\tilde{y}) + \frac{\tilde{z}^2}{2} f_2(\tilde{y}) + \tilde{z} f_3(\tilde{y}) + f_4(\tilde{y}) \tag{35}$$

where $L = (\alpha_0 \alpha \pi^3)/A$. Using the boundary condition $\tilde{W}_2(\tilde{z} = 0) = 0$ we get, $f_4(\tilde{y}) = 0$. Again using the boundary condition $\frac{\partial \tilde{W}_2}{\partial \tilde{z}} \Big|_{\tilde{z}=1/2} = 0$, the function $f_3(\tilde{y})$ is obtained as

$$f_3(\tilde{y}) = -\frac{1}{2} f_2(\tilde{y}) - \frac{1}{8} f_1(\tilde{y}) + \frac{L}{64} \cos(\pi\tilde{y}). \tag{36}$$

After substituting the value of $f_3(\tilde{y})$ and $f_4(\tilde{y})$ in equation (35) we get,

$$\begin{aligned} \tilde{W}_2(\tilde{y}, \tilde{z}) = & -L \cos(\pi\tilde{y}) \left[\frac{\tilde{z}^4}{24} - \frac{\tilde{z}^5}{60} - \frac{\tilde{z}}{64} \right] + \left(\frac{\tilde{z}^3}{6} - \frac{\tilde{z}}{8} \right) f_1(\tilde{y}) \\ & + \left(\frac{\tilde{z}^2}{2} - \frac{\tilde{z}}{2} \right) f_2(\tilde{y}). \end{aligned} \tag{37}$$

Applying the boundary condition $\tilde{W}_2(\tilde{z} = 1) = 0$ we have founded the exact form of $f_1(\tilde{y}) = \frac{9}{40}L \cos(\pi\tilde{y})$. Then the solution expressed as,

$$\begin{aligned} \tilde{W}_2(\tilde{y}, \tilde{z}) = & -L \cos(\pi\tilde{y}) \left[\frac{\tilde{z}^4}{24} - \frac{\tilde{z}^5}{60} - \frac{\tilde{z}}{64} \right] + \frac{9}{40}L \cos(\pi\tilde{y}) \left(\frac{\tilde{z}^3}{6} - \frac{\tilde{z}}{8} \right) \\ & + \left(\frac{\tilde{z}^2}{2} - \frac{\tilde{z}}{2} \right) f_2(\tilde{y}). \end{aligned} \tag{38}$$

Finally, to determine $f_2(\tilde{y})$, the condition $\tilde{W}_2(|\tilde{y}| = (2m + 1)/2) = 0$ being used. It gives that $f_2(\tilde{y})$ satisfies the condition, $f_2\left(\frac{2m+1}{2}\right) = 0$ for $m = 0, 1, 2, 3, \dots$. Following the forms of other terms and satisfying this condition, $f_2(\tilde{y})$ is approximated as, $f_2(\tilde{y}) = FL \cos(\pi\tilde{y})$, where F is determined from the experimental observation. Finally we get the solution of the sub-problem (I) in the following format,

$$\begin{aligned} \tilde{W}_2(\tilde{y}, \tilde{z}) = & -L \cos(\pi\tilde{y}) \left(\frac{\tilde{z}^4}{24} - \frac{\tilde{z}^5}{60} - \frac{\tilde{z}}{64} \right) + \frac{9}{40}L \cos(\pi\tilde{y}) \left(\frac{\tilde{z}^3}{6} - \frac{\tilde{z}}{8} \right) \\ & + FL \cos(\pi\tilde{y}) \left(\frac{\tilde{z}^2}{2} - \frac{\tilde{z}}{2} \right). \end{aligned} \tag{39}$$

A.2.2. Detailed solution of sub-problem II. Using the separation of variables the function $\tilde{W}_1(\tilde{y}, \tilde{z})$ is decomposed as $\tilde{W}_1(\tilde{y}, \tilde{z}) = Y(\tilde{y})Z(\tilde{z})$ where $Y(\tilde{y})$ is a function of \tilde{y} and $Z(\tilde{z})$ is a function \tilde{z} . Therefore equation (17) is expressed as

$$A \frac{\partial^4 (Y(\tilde{y})Z(\tilde{z}))}{\partial \tilde{z}^4} + B \frac{\partial^2 Y(\tilde{y})}{\partial \tilde{y}^2} \frac{\partial^2 Z(\tilde{z})}{\partial \tilde{z}^2} + A \frac{\partial^4 (Y(\tilde{y})Z(\tilde{z}))}{\partial \tilde{y}^4} = 0. \tag{40}$$

The generation and propagation of secondary currents in wide open-channels depends on the variation of bed roughness or bed elevation along lateral direction Wang and Cheng (2005), Kundu and Ghoshal (2014). These lateral change in bed roughness or bed elevation can occur in a periodic manner Yang *et al* (2012), Kundu and Ghoshal (2014). Therefore it can be assumed that the function $Y(\tilde{y})$ changes in a periodic manner along lateral direction and $Y''(\tilde{y}) = \beta_1 Y(\tilde{y})$. Similarly, from the boundary conditions mentioned in Kotsovinos Kotsovinos (1988), further it is assumed that $Z''(\tilde{z}) = \beta_2 Z(\tilde{z})$. Here β_1 and β_2 are some scaling factors. The experimental observations of Wang and Cheng (2006) shows that the variation of vertical and lateral components of secondary current changes in a periodic manner. Therefore the values of β_1 and β_2 can be chosen as $-\pi^2$. These assumptions are in consistent with the experiments of Wang and Cheng (2005) and Wang and Cheng (2006) and observations of Yang *et al* (2012). Therefore equation (40) can be expressed as

$$\frac{Z''}{Z} = -\frac{\beta_1 A Y''}{A\beta_2 Y + B Y''} = -\theta^2 \tag{41}$$

where each ratio is assumed to be equal to $-\theta^2$ ($\theta > 0$) and $2A + B \neq 0$. Then the differential equations with single variables of the functions Y and Z with boundary conditions can be expressed as

$$Z''(\tilde{z}) + \theta^2 Z(\tilde{z}) = 0; \quad Z(\tilde{z} = 0) = 0, \quad Z(\tilde{z} = 1) = 0 \tag{42}$$

and

$$Y'' + \left(\frac{A\beta_2\theta^2}{B\theta^2 - \beta_1A} \right) Y = 0; \quad Y(\tilde{y} = (2m + 1)/2) = 0. \tag{43}$$

The solution of equation (42) is expressed as

$$Z(\tilde{z}) = D_1 \cos(\theta\tilde{z}) + D_2 \sin(\theta\tilde{z}). \tag{44}$$

Using boundary condition in equation (42), one get $D_1 = 0$ and $D_2 \sin(\theta) = 0$. For a non-zero solution, D_2 cannot be zero, therefore we get $\theta_n = n\pi$ in which $n = 1, 2, 3, \dots$. Therefore the function Z which satisfies equation (42) can be written as

$$Z_n(\tilde{z}) = D_2 \sin(n\pi\tilde{z}). \tag{45}$$

Following Kotsovinos (1988), on the onset of instability, $n = 1$ is assumed. Similarly, the solution of equation (43) is expressed as

$$Y(\tilde{y}) = D_3 \cos(\chi_1\tilde{y}) + D_4 \sin(\chi_1\tilde{y}) \tag{46}$$

where $\chi_1 = \sqrt{\left(\frac{A\beta_2\theta_1^2}{B\theta_1^2 - \beta_1A} \right)}$. From the boundary conditions in equation (43), one get $D_4 = -D_3 \frac{\cos\left\{\chi_1\left(\frac{2m+1}{2}\right)\right\}}{\sin\left\{\chi_1\left(\frac{2m+1}{2}\right)\right\}}$. Then the solution $Y(\tilde{y})$ is expressed using the symmetric condition as

$$Y(\tilde{y}) = \frac{D_3}{\sin\left\{\chi_1\left(\frac{2m+1}{2}\right)\right\}} \sin\left\{\left(\frac{2m+1}{2} - |\tilde{y}|\right)\chi_1\right\}. \tag{47}$$

Therefore the final solution $\tilde{W}_1(\tilde{y}, \tilde{z})$ is expressed as

$$\tilde{W}_1(\tilde{y}, \tilde{z}) = C_1 \frac{\sin(\pi\tilde{z})}{\sin\left\{\chi_1\left(\frac{2m+1}{2}\right)\right\}} \sin\left\{\left(\frac{2m+1}{2} - |\tilde{y}|\right)\chi_1\right\} \tag{48}$$

where $C_1 = D_2D_3$ and consequently the final solution $\tilde{r}(\tilde{y}, \tilde{z})$ is expressed as

$$\begin{aligned} \tilde{r}(\tilde{y}, \tilde{z}) = \lambda_* \left[-L \cos(\pi\tilde{y}) \left(\frac{\tilde{z}^4}{24} - \frac{\tilde{z}^5}{60} - \frac{\tilde{z}}{64} \right) + \frac{9}{40} L \cos(\pi\tilde{y}) \left(\frac{\tilde{z}^3}{6} - \frac{\tilde{z}}{8} \right) \right. \\ \left. + FL \cos(\pi\tilde{y}) \left(\frac{\tilde{z}^2}{2} - \frac{\tilde{z}}{2} \right) \right] + C_1 \frac{\sin(\pi\tilde{z})}{\sin\left\{\chi_1\left(\frac{2m+1}{2}\right)\right\}} \\ \times \sin\left\{\chi_1\left(\frac{2m+1}{2}\right)\right\} \sin\left\{\left(\frac{2m+1}{2} - |\tilde{y}|\right)\chi_1\right\}. \tag{49} \end{aligned}$$

To find the constant C_1 , the boundary condition $\tilde{r}(\tilde{y}, \tilde{z}) \Big|_{|\tilde{y}|=2m+1, \tilde{z}=1/2} = \tilde{W}_{\max}$ is substituted into equation (51) which gives

$$C_1 = \lambda_* L \left(\frac{7}{1920} + \frac{F}{8} \right) - \tilde{W}_{\max} \tag{50}$$

Hence, the final solution for the vertical velocity component can be expressed as,

$$\begin{aligned} \tilde{r}(\tilde{y}, \tilde{z}) = \lambda_* & \left[-L \cos(\pi \tilde{y}) \left(\frac{\tilde{z}^4}{24} - \frac{\tilde{z}^5}{60} - \frac{\tilde{z}}{64} \right) + \frac{9}{40} L \cos(\pi \tilde{y}) \left(\frac{\tilde{z}^3}{6} - \frac{\tilde{z}}{8} \right) \right. \\ & \left. + FL \cos(\pi \tilde{y}) \left(\frac{\tilde{z}^2}{2} - \frac{\tilde{z}}{2} \right) \right] + \left[\lambda_* L \left(\frac{7}{1920} + \frac{F}{8} \right) - \tilde{W}_{\max} \right] \\ & \times \frac{\sin(\pi \tilde{z})}{\sin \left\{ \chi_1 \left(\frac{2m+1}{2} \right) \right\}} \sin \left\{ \left(\frac{2m+1}{2} - |\tilde{y}| \right) \chi_1 \right\}. \end{aligned} \tag{51}$$

The transverse velocity component can be obtained from equation (1) after the integration with respect to \tilde{y} as

$$\begin{aligned} \tilde{q}(\tilde{y}, \tilde{z}) = \lambda_* & \left[(L/\pi) \sin(\pi \tilde{y}) \left(\frac{\tilde{z}^3}{6} - \frac{\tilde{z}^4}{12} - \frac{1}{64} \right) - \frac{9}{40} (L/\pi) \sin(\pi \tilde{y}) \left(\frac{\tilde{z}^2}{2} - \frac{1}{8} \right) \right. \\ & \left. - (FL/\pi) \sin(\pi \tilde{y}) \left(\tilde{z} - \frac{1}{2} \right) \right] + \left[\lambda_* L \left(\frac{F}{8} + \frac{7}{1920} \right) - \tilde{W}_{\max} \right] \\ & \times \frac{\pi \cos(\pi \tilde{z})}{\chi_1 \sin \left\{ \chi_1 \left(\frac{2m+1}{2} \right) \right\}} I_* + \Theta(\tilde{z}) \end{aligned} \tag{52}$$

where

$$I_* = \begin{cases} -\cos \left[\chi_1 \left(\frac{2m+1}{2} - |\tilde{y}| \right) \right] & \text{when } \tilde{y} > 0, \\ \cos \left[\chi_1 \left(\frac{2m+1}{2} - |\tilde{y}| \right) \right] & \text{when } \tilde{y} < 0 \end{cases} \tag{53}$$

and $\Theta(\tilde{z})$ is the integration constant and can be determined using the condition $\tilde{q}(\tilde{y} = \pm m) = 0$ where $m = 0, 1, 2, 3, \dots$. This condition is consistent with the experimental observations of Wang and Cheng (2006). Hence from equation (52) we get

$$\Theta(\tilde{z}) = \begin{cases} \left[\lambda_* L \left(\frac{F}{8} + \frac{7}{1920} \right) - \tilde{W}_{\max} \right] \frac{\pi \cos(\pi \tilde{z})}{\chi_1 \sin \left\{ \chi_1 \left(\frac{2m+1}{2} \right) \right\}} \cos \left(\frac{\chi_1}{2} \right) & \text{when } \tilde{y} > 0, \\ - \left[\lambda_* L \left(\frac{F}{8} + \frac{7}{1920} \right) - \tilde{W}_{\max} \right] \frac{\pi \cos(\pi \tilde{z})}{\chi_1 \sin \left\{ \chi_1 \left(\frac{2m+1}{2} \right) \right\}} \cos \left(\frac{\chi_1}{2} \right) & \text{when } \tilde{y} < 0. \end{cases} \tag{54}$$

The final form of the transverse velocity component is ,

$$\begin{aligned} \tilde{q}(\tilde{y}, \tilde{z}) = \lambda_* & \left[(L/\pi) \sin(\pi \tilde{y}) \left(\frac{\tilde{z}^3}{6} - \frac{\tilde{z}^4}{12} - \frac{1}{64} \right) - \frac{9}{40} (L/\pi) \sin(\pi \tilde{y}) \left(\frac{\tilde{z}^2}{2} - \frac{1}{8} \right) \right. \\ & \left. - (FL/\pi) \sin(\pi \tilde{y}) \left(\tilde{z} - \frac{1}{2} \right) \right] + (-1)^N C_1 \frac{\pi \cos(\pi \tilde{z})}{\chi_1 \sin \left\{ \chi_1 \left(\frac{2m+1}{2} \right) \right\}} \\ & \times \left[\cos \left\{ \chi_1 \left(\frac{2m+1}{2} - |\tilde{y}| \right) \right\} - \cos \left\{ \frac{\chi_1}{2} \right\} \right] \end{aligned} \tag{55}$$

with

$$N = \begin{cases} 0 & \text{when } \tilde{y} < 0, \\ 1 & \text{when } \tilde{y} > 0. \end{cases} \quad (56)$$

ORCID iDs

Snehasis Kundu  <https://orcid.org/0000-0003-3222-2022>

Titas Chattopadhyay  <https://orcid.org/0000-0002-8338-4788>

References

- Absi R 2010 Concentration profiles for fine and coarse sediments suspended by waves over ripples: an analytical study with the 1-dv gradient diffusion model *Adv. Water Resour.* **33** 411–18
- Bradshaw P 1987 Turbulent secondary flows *Ann. Rev. Fluid Mech.* **19** 53–74
- Brundrett E and Baines W D 1964 The production and diffusion of vorticity in duct flow *J. Fluid Mech.* **19** 375–94
- Chiu C L and Chou J D 1985 Flow-shear interaction in rectangular open channels *Proc. of 21st IAHR Congress (Melbourne)* pp 87–91
- Chiu C L and Lin G F 1983 Computation of 3-d flow and shear in open channel *J. Hydraul. Div. ASCE* **109** 1424–40
- Coleman J 1969 Brahmaputra river; channel process and sedimentation *Sediment. Geol.* **3** 129–239
- Coleman N 1981 Velocity profiles with suspended sediment *J. Hydraul. Res.* **19** 211–29
- Francis J 1878 On the cause of the maximum velocity of water flowing in open channels being below the surface *Trans. Am. Soc. Civil Eng.* **7** 109–13
- Gessner F B and Emery A F 1981 The numerical prediction of developing turbulent flow in rectangular ducts *J. Fluid Eng. ASME* **103** 445–54
- Gessner F 1973 The origin of secondary flow in turbulent flow along a corner *J. Fluid Mech.* **58** 1–25
- Ghoshal K, Mazumder R, Chakraborty C and Mazumder B 2013 Turbulence, suspension and downstream fining over a sand gravel mixture bed *Int. J. Sediment. Res.* **28** 194–209
- Gibson A 1909 On the depression of the filament of maximum velocity in a stream flowing through an open channel *Proc. R. Soc. A* **82** 149–59
- Gordon L 1992 *Mississippi River Discharge* (San Diego: RD Instruments)
- Guo J 1998 Turbulent velocity profile in clear water and sediment-laden flows *PhD Thesis* Colorado State University, Fort Collins, CO
- Guo J 2006 Self-similarity of mean flow in pipe turbulence *36th AIAA Fluid Dynamics Conferences and Exhibit (San Francisco, CA)* AIAA Paper 2885
- Guo J and Julien P 2001 Turbulent velocity profiles in sediment-laden flows *J. Hydraul. Res.* **39** 11–23
- Guo J and Julien P 2008 Application of the modified log-wake law in open-channels *J. Appl. Fluid Mech.* **1** 17–23
- Hallez Y and Magnaudet J 2009 Turbulence-induced secondary motion in a buoyancy-driven flow in a circular pipe *Phys. Fluids* **21** 081704
- Hinze J 1975 *Turbulence* (New York: McGraw-Hill)
- Ikeda S 1981 Self forced straight channels in sandy beds *J. Hydraul. Div.* **107** 389–406
- Immamoto H and Ishigaki T 1988 Measurement of secondary flow in an open channel *Proc. 6th IAHR-APD Congress* pp 513–20
- Kinoshita R 1967 An analysis of the movement of flood waters by aerial photography; concerning characteristics of turbulence and surface *Photogr. Surv.* **6** 1–17 in Japanese
- Kotsovinos N E 1988 Secondary currents in straight wide channels *Appl. Math. Modelling* **12** 22–4
- Kundu S 2015 Theoretical study on velocity and suspension concentration in turbulent flow *PhD Thesis* Indian Institute of Technology Kharagpur, West Bengal, India
- Kundu S 2016 Effect of lateral bed roughness variation on particle suspension in open channels *Environ. Earth Sci.* **75** 1–18
- Kundu S and Ghoshal K 2012 An analytical model for velocity distribution and dip-phenomenon in uniform open channel flows *Int. J. Fluid Mech. Res.* **39** 381–95

- Kundu S and Ghoshal K 2013 Influence of secondary current on vertical concentration distribution in an open channel flow *ISH J. Hydraul. Eng.* **19** 88–96
- Kundu S and Ghoshal K 2014 Effects of secondary current and stratification on suspension concentration in an open channel flow *Environ. Fluid Mech.* **14** 1357–80
- Lin Z W, Shao X M, Yu Z S and Wang L P 2017 Effects of finite-size heavy particles on the turbulent flows in a square duct *J. Hydrodyn.* **29** 272–82
- Lin Z, Yu Z, Shao X and Wang L 2017 Effects of finite-size neutrally buoyant particles on the turbulent flows in a square duct *Phys. Fluids* **29** 103304
- Lu J, Zhou Y, Zhu Y, Xia J and Wei L 2018 Improved formulae of velocity distributions along the vertical and transverse directions in natural rivers with the sidewall effect *Environ. Fluid Mech.* **18**
- McLean S R 1981 The role of non-uniform roughness in the formation of sand ribbons *Mar. Geol.* **42** 49–74
- Moramarcio T S and Singh V P 2004 Estimation of mean velocity in natural channels based on Chiu's velocity distribution equation *J. Hydrol. Eng. ASCE* **9** 42–50
- Nakagawa H, Nezu I and Tsujimoto T 1981 Turbulence structure with and without cellular secondary currents over various bed configurations *Ann. Disaster Prev. Res. Inst. Kyoto Univ.* **24B** 311–38
- Naot D and Rodi W 1982 Calculation of secondary currents in channel flow *J. Hydraul. Div.* **108** 948–68
- Nezu I and Nakagawa H 1984 Cellular secondary currents in straight conduit *J. Hydraul. Eng.* **110** 173–93
- Nezu I and Nakagawa H 1993 *Turbulence in Open-Channel Flows* (Rotterdam: IAHR Monograph)
- Nezu I and Rodi W 1985 Experimental study on secondary currents in open channel flow *21th IAHR Congress (Melbourne)* IAHR pp 115–19
- Perkins H J 1970 The formation of streamwise vorticity in turbulent flow *J. Fluid Mech.* **44** 721–40
- Prandtl L 1926 Über die ausgebildete turbulenz *2e Internationaler Kongress der Technischen Mechanik, Verhandlung (Füessli, Zürich)*
- Proust S and Nikora V 2020 Compound open-channel flows: effect of transverse current on the flow structure *J. Fluid Mech.* **885** 1–38
- Soualmia A, Zaouali S and Labiod C 2008 Modeling of secondary motions driven by the turbulence anisotropy in closed and open channels *Lebanese Sci. J.* **9** 75–89
- Stearns F 1883 On the current-meter: together with a reason why the maximum velocity of water flowing in open channel is below the surface *Trans. Am. Soc. Civil Eng.* **12** 301–38
- Thomson J 1876 On the origin of windings of rivers in alluvial plains, with remarks on the flow of water round bends in pipes *Proc. R. Soc.* **25** 5–8
- Townsend A A 1976 *The Structure of Turbulent Shear Flow* (Cambridge: Cambridge University Press)
- Tracy H 1965 Turbulent flow in a three dimensional channel *J. Hydraul. Div. ASCE* **6** 9–35
- Vanoni V 1946 Transportation of suspended sediment by running water *Trans. ASCE* **111** 67–133
- Wang Z and Cheng N 2005 Secondary flows over artificial bed strips *Adv. Water Resour.* **28** 441–50
- Wang Z and Cheng N 2006 Time-mean structure of secondary flows in open channel with longitudinal bedforms *Adv. Water Resour.* **29** 1634–49
- Wang Z and Cheng N 2008 Influence of secondary flow on distribution of suspended sediment concentration *J. Hydraul. Res.* **46** 548–52
- Yalin M 1977 *Mechanics of Sediment Transport* 2nd edn (New York: Pergamon Press)
- Yang S Q 2005 Interactions of boundary shear stress, secondary currents and velocity *Fluid Dyn. Res.* **36** 121–36
- Yang S Q, Tan S K and Wang X K 2012 Mechanism of secondary currents in open channel flows *J. Geophys. Res.* **117** 1–13
- Yang S 2007 Turbulent transfer mechanism in sediment-laden flow *J. Geophys. Res.* **112** 1–14
- Yang S, Tan S and Lim S 2004 Velocity distribution and dip-phenomenon in smooth uniform open channel flows *J. Hydraul. Eng.* **130** 1179–86